AGU PUBLICATIONS

JGR

Journal of Geophysical Research: Atmospheres

RESEARCH ARTICLE

10.1002/2013JD020781

The 2010 eruption of Eyjafjallajökull: Lightning and plume charge structure

S. A. Behnke[1], R. J. Thomas[1], H. E. Edens[1], P. R. Krehbiel[1], and W. Rison[1]

[1]Langmuir Laboratory, New Mexico Institute of Mining and Technology, Socorro, New Mexico, USA

Key Points:
- Monopolar and dipolar charge structures were inferred
- Vent charging was the dominant mechanism
- Volcanic ejecta carried net positive charge

Correspondence to:
S. A. Behnke,
sonjabehnke@usf.edu

Citation:
Behnke, S. A., R. J. Thomas, H. E. Edens, P. R. Krehbiel, and W. Rison (2014), The 2010 eruption of Eyjafjallajökull: Lightning and plume charge structure, *J. Geophys. Res. Atmos.*, *119*, doi:10.1002/2013JD020781.

Received 22 AUG 2013
Accepted 18 DEC 2013
Accepted article online 19 DEC 2013

Abstract Six Lightning Mapping Array (LMA) stations were deployed in April 2010 around Eyjafjallajökull volcano in southern Iceland. Single-station LMA observations were made during the first explosive period (14–18 April), and three-dimensional LMA observations were made during the second explosive period (5–22 May). The single-station observations revealed that continuous RF electrical activity caused by high rates of small vent discharges occurred during the first explosive period, but not the second, indicating that the strength of vent charging varied between the first and second explosive periods. During the second explosive period, very little lightning was detected between 5 and 10 May, while moderate rates of lightning were detected between 11 and 21 May, signaling that another change occurred on 11 May that affected plume electrification. The data do not make clear if it was changing eruptive activity or changing meteorological activity that resulted in the sudden onset of lightning. The plume charge structure during the second explosive period was inferred from the three-dimensional lightning data, showing that the dominant charge structure varied between a positive monopole and a negative-over-positive dipole. The predominance of a low-altitude region of positive charge and the observation that electrical activity was concentrated near the vent indicate that net positive vent charging was dominating the electrification.

1. Introduction

Charging of volcanic plumes can be caused by several mechanisms that occur either proximally to the vent or at altitude in the plume. The proximal mechanisms are those that generate charge as an immediate consequence of the eruption of magma, such as fracture charging of silicate particles, contact electrification of silicate particles, and boiling of fresh or salt water upon contact with magma. Mechanisms that occur secondary to the eruption within the plume include contact electrification of silicate particles and thunderstorm-style plume-based ice-contact charging. A thorough review of the various mechanisms is provided by *James et al.* [2008].

Of interest in volcanic lightning studies is the degree to which the various charging mechanisms electrify volcanic plumes and produce lightning in the plumes. It has been shown that the proximal, silicate-based mechanisms (collectively referred to herein as vent charging) can produce intense lightning at the vent of a volcano [*Thomas et al.*, 2007, 2010], while thunderstorm-style plume-based ice-contact charging contributes to the extensive amounts of lightning that have been observed higher up in the plumes both above and downwind of the vent following an explosive eruption [*Behnke et al.*, 2013]. Three-dimensional lightning mapping observations can be used to infer the dominant charge structure in the plume, utilizing methods previously developed for thunderstorms [e.g., *Thomas et al.*, 2002; *Marshall et al.*, 2005; *Rust et al.*, 2005; *Krehbiel et al.*, 2008], which can provide insight into the charging mechanisms.

Use of the charge identification method to investigate charge structure and its evolution has been done many times on thunderstorms [e.g., *Wiens et al.*, 2005; *Tessendorf et al.*, 2007a; *Bruning et al.*, 2010] and is now, for the first time, applied to volcanic plumes. This study presents lightning observations from the 2010 eruption of Eyjafjallajökull, with an emphasis on three-dimensional data obtained during the latter part of the eruption (1–22 May) to determine both the dominant charge structure and the relative roles of the various charging mechanisms in producing and affecting the electrification. Regions of positive and negative charge are identified showing that the charge structure varied between monopolar and dipolar structures throughout the eruption. Overall, the observations indicate that silicate-based vent charging was the dominant mechanism.

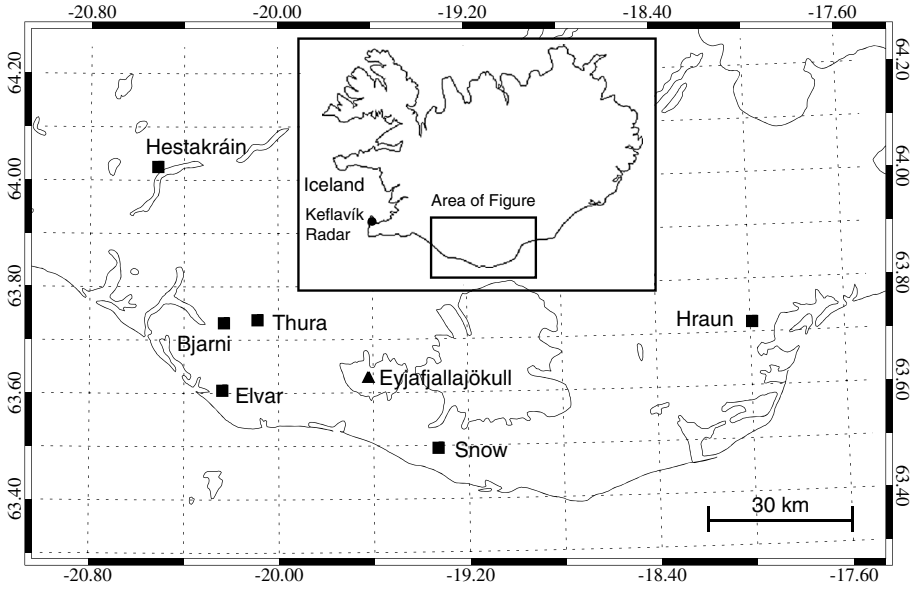

Figure 1. Map showing the locations and names of the six lightning mapping stations in southern Iceland (squares) and the approximate location of the summit crater of Eyjafjallajökull (triangle). The location of the Keflavík radar is shown in the inset.

2. Data and Methods

2.1. Lightning Mapping Array Data

The Lightning Mapping Array (LMA) is a network of very high frequency (VHF) receiving stations that locate radiation sources produced by lightning [*Rison et al.*, 1999; *Thomas et al.*, 2004]. Each station records impulsive VHF emissions generated by lightning as it develops. Global Positioning System (GPS) timing is used to record the arrival time of the peak power of the VHF signal in successive 10 or 80 μs time windows when the signal exceeds a local noise threshold. Time-of-arrival methods are used to determine the locations and times of the radiation sources.

A six-station Lightning Mapping Array (LMA) was deployed in southern Iceland in April 2010 (Figure 1) shortly after the onset of the explosive eruption of Eyjafjallajökull on 14 April. All six stations were operational by 1 May, though individual station observations were obtained starting on 15 April. In this deployment, five stations operated in the 60–66 MHz band and the sixth station operated at 54–60 MHz due to local interference in the 60–66 MHz band. Data were collected in 10 μs mode for maximum detection of the lightning activity.

The data were processed by requiring a minimum of five of the six stations to participate in the solutions of the location and origin time of the radiation sources. The RMS uncertainties in the *x*, *y*, and *z* positions of the non-noise contaminated source locations were calculated to be on the order of 10, 20, and 200 m, respectively [see *Thomas et al.*, 2004]. To limit the influence of random noise (chance correlations of the data that tend to be poorly located with respect to the actual lightning sources) and noise-affected solutions in the subsequent analysis of the processed data, each processed data set was pared down by limiting the extent of the data in latitude, longitude, and altitude and by additionally restricting the goodness of fit (χ_ν^2) values of the located sources. This filtering of the located data is described in Appendix A.

Flash rates and locations of flash initiation were determined using the flash algorithm included in XLMA, the LMA data visualization software utilized in the analyses [*Thomas et al.*, 2003]. The algorithm groups individual sources with other sources if the temporal and spatial separation between them is within specified limits. The flash algorithm considers only the horizontal separation between sources; the altitude of the sources is not used because of the larger uncertainties associated with altitude. In this study, values of 3000 m and 150 ms were used for the maximum spatial and temporal separation allowed between individual sources in a flash. Only groupings of three or more sources were considered to be flashes. From these groupings, clusters of 10 or more sources were classified as "regular" discharges and clusters of three to nine sources were classified as "small" discharges. Single-source and two-source clusters were ignored to avoid inclusion of

isolated noise solutions (even after filtering the data as described in Appendix A, there was still a significant number of noise solutions in the data). The decision to use 10 sources as the dividing line between regular and small discharges was arbitrary, though the 10-source threshold is commonly used in thunderstorm studies for calculating flash rates [e.g., *Wiens et al.*, 2005; *Tessendorf et al.*, 2007a, 2007b]. Thunderstorm studies typically ignore clusters with fewer than 10 sources to limit the influence of noise solutions on the flash rate; however, in this study clusters of three to nine sources have been included because manual inspection of the data has shown that there were many well-located small clusters of VHF sources in addition to the larger clusters. *Wiens et al.* [2005] compared the sensitivity of a 10-, 50-, and 100-source threshold on flash rate and found that using higher thresholds still preserved the trends in the flash rate, though the flash rates themselves were severely diminished. A 10-source threshold for regular discharges was used in this study to allow the flash rates to be comparable to other LMA studies.

In this article the terms "flash" and "discharge" are used interchangeably to mean a lightning discharge of any size. The terms "small discharge" and "regular discharge" are used to specifically describe the two types of discharges identified by the flash algorithm, as explained above. Altitudes of flashes or VHF sources given in this article correspond to altitude above mean sea level (msl).

2.1.1. Charge Structure Analysis

The process of identifying regions of net charge is entirely manual and relies on three insights: (i) the LMA primarily detects negative polarity breakdown, (ii) negative and positive polarity breakdown differ in their appearance and development, and (iii) lightning leaders propagate into and through regions of net charge. These considerations, discussed in more detail below, were used to infer the dominant charge regions in the plume of Eyjafjallajökull.

It has been found that negative polarity breakdown radiates more strongly than positive breakdown at VHF [e.g., *Shao and Krehbiel*, 1996]. As a result, it can be assumed that most of the activity mapped by the LMA comes from negative breakdown. Since positive breakdown is typically not detected directly, its location is usually inferred from the occurrences of fast negative polarity leaders (also referred to as K-events, recoil leaders, or retrograde negative breakdown), which propagate back along the positive leader channel toward the negative end. The VHF emissions from these secondary negative leaders reveal the paths of positive leader channels. It is possible, however, for the LMA to detect positive breakdown of virgin air in the absence of negative polarity breakdown [*Edens et al.*, 2012].

The located VHF sources can be used to infer regions of net positive or negative charge due to the characteristic appearance that positive and negative polarity leaders display when mapped with the LMA [e.g., *Rust et al.*, 2005; *Bruning et al.*, 2010]. Negative breakdown mapped by the LMA due to the initial breakdown of virgin air has a somewhat "noisy" appearance compared to positive breakdown mapped by the LMA due to secondary negative breakdown, which has a more filamentary appearance. In addition, the amplitude of the source power can be used to confirm inferences made based on channel appearance. Typically, the radiation events with the highest source powers come from the negative end of the bidirectional channels, though low source power events exist along both leader polarities [*Thomas et al.*, 2001].

The identification of positive or negative breakdown due to the characteristics described above generally leads to the inference of a charge region of the opposite polarity, as lightning tends to propagate into and through regions of net charge [*Coleman et al.*, 2003; *Riosset*, 2007; *Williams et al.*, 1985]. For example, in a typical intracloud discharge occurring in a dipole or tripole charge structure, the negative end of the bipolar leader will first propagate vertically toward a positive charge layer and then horizontally within the positive layer, while the positive end does the opposite. The horizontal parts of the leader channels typically indicate that a region of net charge exists there, while the vertical parts may indicate the presence of a neutral region or a region with a sufficiently strong vertical electric field that would suppress horizontal branching. This method locates the charge regions in a cloud or plume that lightning is propagating in, giving an overall picture of the charge structure.

2.2. ATDnet Data

The UK Met Office operates a very low frequency lightning location network called ATDnet, which is optimized to detect lightning in Europe [*Bennett et al.*, 2010]. At the time of the eruption, there was one ATDnet station in Iceland. The network stations primarily detect sferics from cloud-to-ground discharges. Intracloud discharges may also be detected, but sensitivity is limited, especially at long ranges. ATDnet does not attempt to distinguish between cloud-to-ground and intracloud discharges, and the polarity of the

discharges is not determined. The typical location uncertainty is 3 km, and the network detects an estimated 60% of discharges in Iceland with peak current higher than 15 kA. ATDnet detected 790 discharges near Eyjafjallajökull during the entire eruption [*Bennett et al.*, 2010].

ATDnet data were used in this study to help determine if a discharge mapped by the LMA was a cloud-to-ground discharge. Though ATDnet does not discriminate between intracloud and cloud-to-ground discharges, in this analysis it has been assumed that most of the sferics detected by ATDnet were from return strokes of cloud-to-ground flashes. This was also assumed by *Bennett et al.* [2010]. The relative timing between ATDnet detection and the VHF sources detected by the LMA was used in some circumstances to help infer the polarity of a cloud-to-ground discharge, which was useful for understanding the nature of the electrical activity as a whole. In particular, if an ATDnet event was detected before the LMA detected any radiation sources, it was assumed that ATDnet detected the return stroke of a positive cloud-to-ground discharge since the LMA would likely not have detected radiation from its weakly radiating positive leader to ground.

2.3. Plume Height Data

Plume height measurements were obtained throughout the eruption by a C-band weather radar located at the Keflavík International Airport, approximately 155 km from the volcano [*Arason et al.*, 2011a]. Full volume reflectivity scans (a total of 12 elevation angles out to 240 km range) were made in 5 min intervals during the eruption, except at 5 and 35 min past each hour when Doppler scans with a range of 120 km were made. An echo top algorithm was used to determine the plume top altitude, reported in this article as altitude above mean sea level (msl). The lowest detectable cloud height over Eyjafjallajökull was 2.9 km due to blockage of the lowest beam by an intervening mountain range; however, if the plume was detectable only by the lowest beam, the plume altitude was reported as 2.8 km, corresponding to the center of the beam. The 5 min data were averaged over time periods of 1, 3, 6, 12, and 24 h. The 1 h averaged time series of the plume height from 14 April to 22 May is presented in Figure 2b [*Arason et al.*, 2011b]. Gaps in the time series were the result of missing data or because the plume was either below the detectable limit (2.9 km) or obscured by meteorological clouds.

The beamwidth, range, and scanning strategy contributed to the plume height uncertainties. As range increases, so does the vertical distance between elevation angles. The five lowest scan angles were 0.5, 0.9, 1.3, 2.4, and 3.5°, corresponding to beam midpoint altitudes of 2.8, 3.9, 4.9, 7.9, and 10.9 km at the distance of the volcano. The half-power beamwidth was 0.9°, corresponding to a width of 2.4 km at the range of Eyjafjallajökull. The beams overlap only for the three lowest elevation angles.

2.4. Meteorological Data

The variation of local winds and the atmospheric temperature structure around Eyjafjallajökull during the eruption were obtained from *Arason et al.* [2011c], who procured the data from the UK Met Office's Unified Model. As described by *Arason et al.* [2011c], the Unified Model (UM) is a numerical modeling software package used by the Met Office for forecasting. The Numerical Atmospheric-dispersion Modeling Environment (NAME) package, which was also developed by the UK Met Office, was used to linearly interpolate the meteorological data from the UM to the location of Eyjafjallajökull between altitudes of 1667 m (the assumed summit altitude) and 10,167 m at 100 m intervals. The wind and temperature data are reproduced in Figures 2b–2d.

3. Volcanic Plume Charging Mechanisms

Previous lightning mapping observations of electrical activity during explosive volcanic eruptions have demonstrated that volcanic ejecta are charged upon exiting the volcano. Lightning mapping observations obtained during explosive eruptions of Mount St. Augustine (Alaska, 2006) showed that vigorous small electrical discharges called vent discharges occurred at the vent of the volcano as ash and gas were being erupted from the vent, indicating that the ejecta were charged upon eruption [*Thomas et al.*, 2007, 2010]. The vent discharges were so intense that the radiation they produced looked continuous to the LMA (the rate of recorded VHF events was greater than 1 per millisecond typically over periods of 30 s or more). The unique VHF signature of this activity is referred to as continuous RF radiation. Continuous RF was also observed during the explosive eruptions of Redoubt Volcano (Alaska, 2009), corroborating the Augustine results that the ejecta from explosive volcanic eruptions are charged [*Behnke et al.*, 2013].

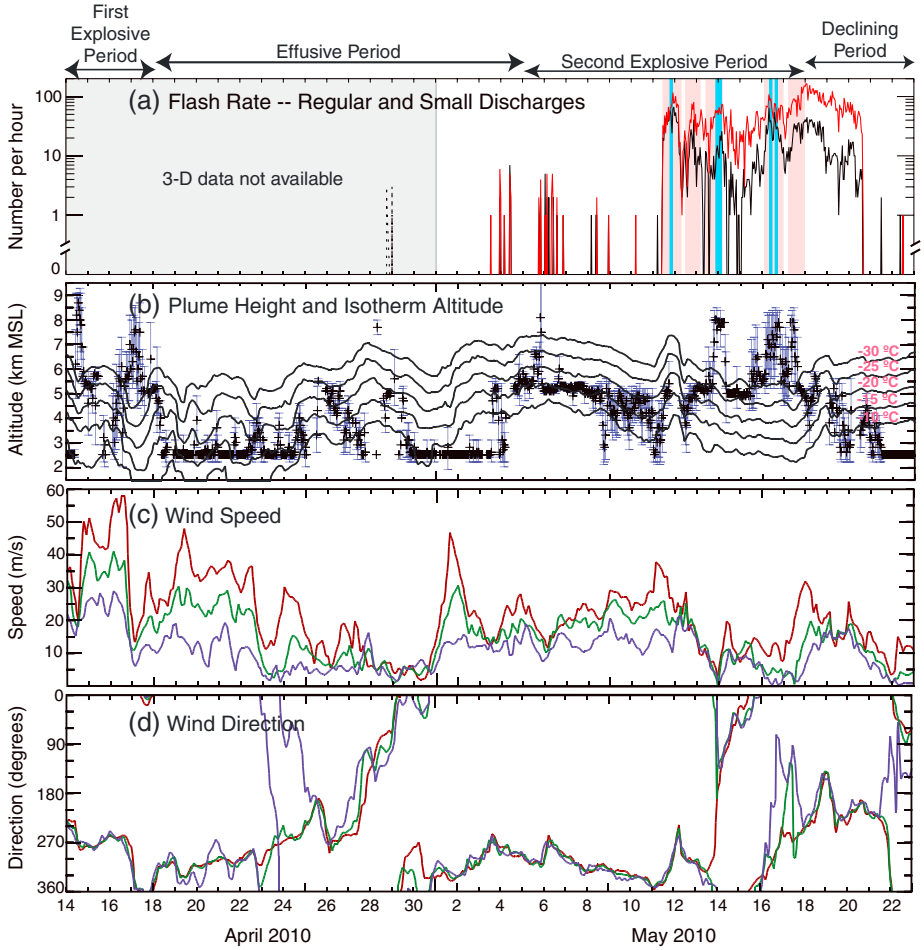

Figure 2. Overview of lightning rates, radar-derived plume heights, and the meteorological conditions present during the four phases of eruptive activity (arrows at top of figure) inferred by *Gudmundsson et al.* [2012] during the 2010 eruption of Eyjafjallajökull. (a) Hourly rates of regular discharges (black line) and small discharges (red line) determined from the three-dimensional data shown on a logarithmic scale. Hourly rates of discharges determined from two-station data during the effusive phase are indicated by the black dotted line. Pink and blue shaded areas indicate times when either a monopolar or dipolar charge structure was observed. White areas indicate times when either no lightning occurred or the charge structure was indeterminable. (b) One hour averages and standard deviations of the radar-derived plume heights and altitudes of the −10, −15, −20, −25, and −30°C isotherms. (c) Wind speed and (d) direction at Eyjafjallajökull at 3 (blue line), 5 (green line), and 7 km (red line) altitudes. The isotherm (Figure 2b) and wind plots (Figures 2c and 2d) were adapted from *Arason et al.* [2011c]. Copyright 2011 American Geophysical Union. Reproduced/modified by permission of American Geophysical Union.

The observational evidence of charged volcanic ejecta is supported by laboratory studies, which have shown that silicate particles are imparted with a net charge when they are subjected to brittle fracture [*James et al.*, 2000]. During eruption, magma is fractured into tephra by the expansion of volcanic gas. Charging due to fracture is believed to be caused by fractoemission, a process in which charged particles (electrons and ions) are ejected as a result of material fracture [*Dickinson et al.*, 1988]. Laboratory investigation of the fracture charging mechanism has shown that the silicate particles produced through fracture carry a net charge with a magnitude similar to what had been previously measured on charged ashfall [*James et al.*, 2000]. In the experiments, both positively and negatively charged particles were produced, but a small imbalance of charge existed. Most sample types produced particles with net negative charge, except for the most silica-poor sample, which produced particles with net positive charge. The emitted charge is believed to be carried on ions escaping from the fractured surfaces. A metal mesh was placed above the fracturing apparatus during the experiments, which detected a charge opposite to that detected on the silicate particles. During an eruption, ions released from fractured surfaces would be expected to quickly attach to larger particles, such as other silicate particles, cloud particles, and the vent of the volcano. Some researchers, who have inferred dipolar and tripolar charge structures in small plumes from ground-based

potential gradient measurements, have suggested that charge separation in these plumes was due to silicate particles carrying one net charge and gas (presumably cloud particles, as charged gas molecules would quickly attach to larger particles) carrying the opposite net charge [*Lane and Gilbert*, 1992; *Miura et al.*, 2002].

Charging during the eruption processes is also expected to result from contact electrification of silicate particles. Studies of contact charging on granular materials (for a full review, see *Lacks and Sankaran* [2011]) have shown that there is a size dependence on charge polarity. In particular, researchers have found that larger particles tend to charge positively and smaller particles tend to charge negatively [*Forward et al.*, 2009]. *Houghton et al.* [2013] studied contact charging of volcanic ash using samples from the 2011 eruption of Grímsvötn and found that the span of the particle size distribution affected the amount of charging. Specifically, they found that larger particle distribution spans resulted in more charge separation. This mechanism would be expected to occur both in the vent and throughout the eruption column, as long as the silicate particles remained dry.

Another proximal vent charging process to consider is that which occurs during boiling of fresh or salt water [e.g., *Blanchard*, 1964]. Due to the polar nature of water molecules, charge separation occurs due to mechanical disruption of water during vigorous boiling [*James et al.*, 2008]. This process can occur during volcanic eruptions where there is contact between magma and an external water source. Strong positive charging leading to lightning due to contact between lava and salt water has been observed during the eruptions of Surtsey and Heimaey in Iceland [*Anderson et al.*, 1965; *Brook et al.*, 1974].

In addition to the vent charging processes described above, lightning mapping observations of the 2006 Augustine Volcano and 2009 Redoubt Volcano eruptions showed that subsequent charging in the plume likely played an important role in the production of intracloud lightning in eruption columns produced by large explosive events. Following a relatively large explosive event during the Augustine eruption, lightning was observed in the plume over a period of approximately 12 min as the plume drifted away from the volcano. These discharges occurred after a delay of several minutes of inactivity following the main explosion [*Thomas et al.*, 2007, 2010]. The time delay and the repeated occurrence of lightning in the downwind plume suggest that an in situ charging process was occurring, as opposed to charge advection from the vent. Following the large explosive events of the Redoubt eruption, lightning often persisted for 20 to 70 min within the plumes, which reached altitudes up to 19 km (msl) [*Behnke et al.*, 2013]. Volcanic plumes typically contain large amounts of water [*Sparks et al.*, 1997] that may exceed amounts found in typical thunderstorms [*Williams and McNutt*, 2005], and it was demonstrated that these high altitude plumes would have contained ice or ice-coated silicate particles; thus, contact charging of ice particles, analogous to thunderstorm charging, was likely the dominant mechanism responsible for the prolific amounts of lightning observed during Redoubt's eruption [*Behnke et al.*, 2013].

In summary, charging of volcanic plumes is expected to be caused by a combination of mechanisms. The main goal of this study is to use lightning observations combined with radar and atmospheric data to determine the relative importance of these mechanisms.

4. The Eruption of Eyjafjallajökull

The summit eruption of Eyjafjallajökull occurred between 14 April and 22 May following the small flank eruption that occurred from 20 March to 12 April. The summit eruption consisted of two separate phases of energetic explosive activity (14–18 April and 5–17 May), a period of effusive activity (18 April–5 May) and a final phase of declining explosive activity (17–22 May) (for a complete description, see *Gudmundsson et al.* [2012]). The timing of the four eruptive periods is indicated at the top of Figure 2. From 14 to 18 April, phreatomagmatic explosive activity was observed, which is referred to as the "first explosive period" in the rest of this article. A phreatomagmatic eruption results from the interaction between magma and ground or surface water. After 18 April, eruptive activity decreased and switched to effusion of lava with very limited explosive activity. On 5 May, explosive volcanic activity recommenced with magmatic style activity and is referred to as the "second explosive period." Generally speaking, a magmatic eruption results from expansion and exsolution of volatiles within the magma during, for example, decompression of the magma as it moves from higher to lower pressures. The eruption began to decline on 18 May and explosive activity ended on 22 May.

The 2010 Eyjafjallajökull eruption has been classified as a VEI (volcanic explosivity index) 3 event [*Gudmundsson et al.*, 2012]. VEI is a semiquantitative logarithmic scale ranging from 0 to 8 that is used as a measure of the magnitude of an eruption [*Newhall and Self*, 1982]. The total volume of erupted products and the eruption column height are the primary quantitative measures considered in the classification. *Newhall and Self*, 1982] describe a VEI 3 event as moderate to large event that would be qualitatively described as "explosive." The maximum plume height during the eruption of Eyjafjallajökull was 10 km, and the estimated total volume of erupted material was 0.18 ± 0.05 km^3 (equivalent to $4.8 \pm 1.2 \times 10^{11}$ kg) [*Gudmundsson et al.*, 2012]. Approximately 35% of the total material was erupted during the first explosive period alone, which had a duration of 4 days.

Overall, the erupted tephra consisted of mostly fine ash particles with diameters of less than 1000 μm [*Gudmundsson et al.*, 2012]. Tephra is a general term for fragmented silicate particles; ash particles are tephra particles with a diameter of less than 2 mm. According to [*Gudmundsson et al.*, 2012], a complete grain size analysis has not yet been completed for the entire eruption, but the available observations indicate that the ash from the second explosive period (5–17 May) was less fine than the first explosive period (14–18 April), though ash grain size from both periods are comparable. *Dellino et al.* [2012] showed that ash from the first period was generally blocky and poorly vesiculated (vesicles are bubbles formed during exsolution of dissolved gases) due to the magma-water interaction, while ash from the second period was highly vesicular and had either an angular or irregular shape.

5. Results and Discussion

5.1. Overview of Observations

Though the LMA was not fully operational until 1 May 2010, at least one station was recording data throughout most of the eruption. Single-station observations began on 15 April, and by 19 April, at least two stations were operating at all times. On 1 May, all six stations were operational, providing three-dimensional data (Figure 2a). Though not enough stations were collecting data prior to 1 May to provide three-dimensional lightning locations, the unprocessed data were examined manually, both by visual inspection and using two-station time correlations to determine when lightning occurred.

Single-station LMA observations revealed that both continuous RF and discrete electrical discharges occurred during the first explosive period. Three examples of 10 min of unprocessed data from this period are shown in Figure 3. Each plot in this figure shows a 2-D histogram of the peak VHF power. The colors indicate event density, red being most number of events and purple being least number. The distinct vertical lines in each plot were usually caused by discrete lightning discharges, though they can also be caused by a strong, localized noise source. Typically, the relatively thick lines are produced by large-scale lightning discharges, while the thin, purple-colored lines are from smaller discharges. The continuous-looking signal that is visible in all three examples is caused by continual radio frequency (RF) impulses and is referred to as "continuous" RF electrical activity. It is most prominent in Figure 3b, occurring from approximately 04:32:30 to 04:37:00. This type of electrical activity was previously observed during the 2006 eruption of Augustine Volcano [*Thomas et al.*, 2007, 2010] and the 2009 eruption of Redoubt Volcano [*Behnke et al.*, 2013, 2012], and is the result of high rates of very small "vent discharges" ($\sim$ 10–100 m in length) occurring directly above the vent of the volcano in the eruption column, due to charged volcanic ejecta (section 3). Both continuous RF and discrete lightning discharges were frequently observed throughout the first explosive period during the eruption of Eyjafjallajökull.

The three examples presented in Figure 3 show that the continuous RF activity observed during the first explosive period often varied in intensity. Out of these examples, continuous RF was the strongest (had the highest density of events) between 04:30 and 04:40 UTC, shown in Figure 3b, and was the weakest between 00:20 and 00:30 UTC, shown in Figure 3a. Because the discharges producing continuous RF are caused by charge on volcanic ejecta, the variation in the intensity of the continuous RF suggests that there were variations in the eruptive activity affecting the charging of the ejecta. It is not possible to single out which vent charging mechanisms were causing the continuous RF, but it is worth reiterating that the eruptive activity from the first explosive period was phreatomagmatic; thus, in addition to fracture charging and contact electrification among silicate particles, charging due to boiling of water is also expected to have contributed to the electrification.

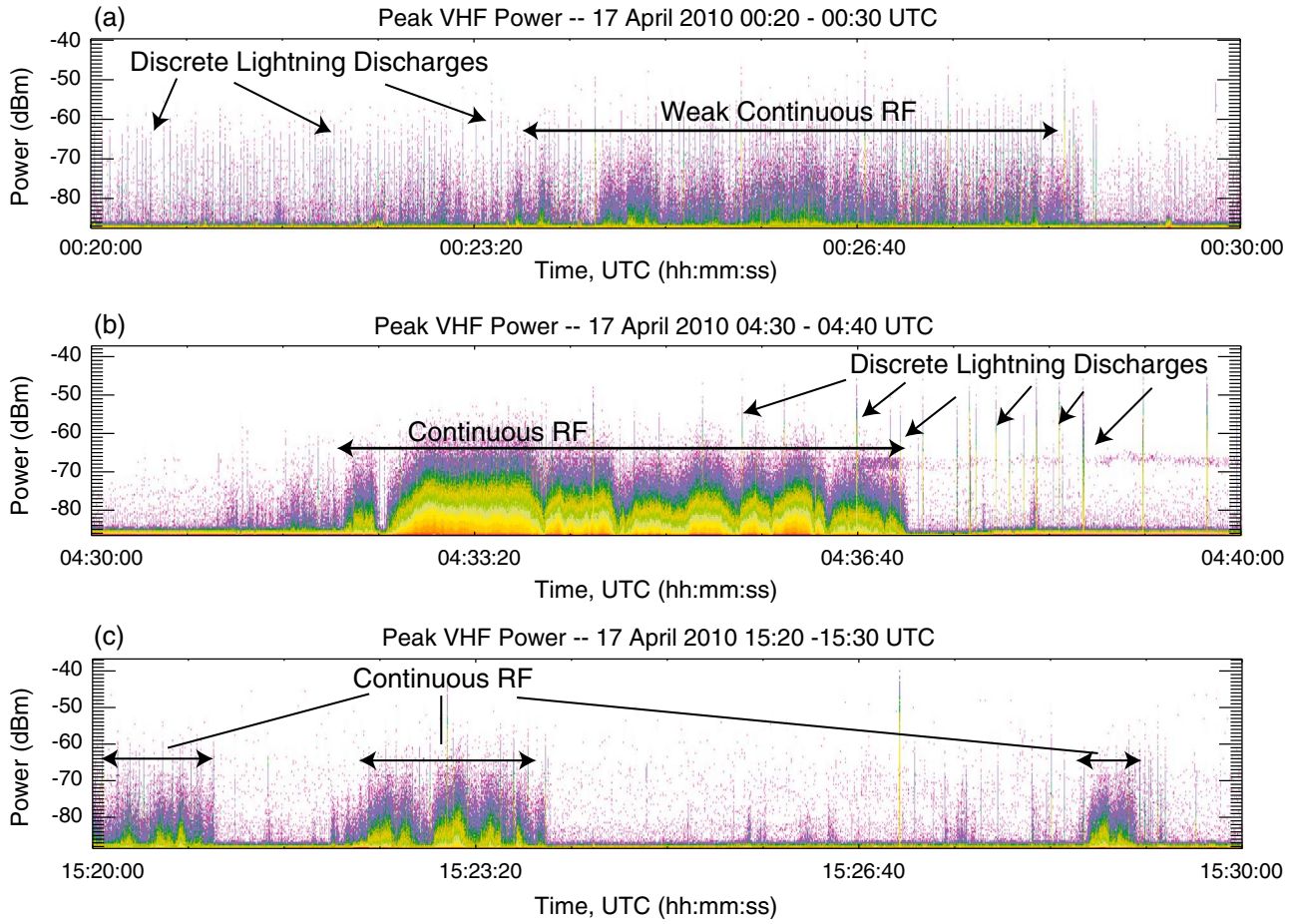

Figure 3. Three examples of unprocessed (raw) data collected by the "Bjarni" station on 17 April 2010. Arrows point to examples of continuous RF and discrete lightning discharges (though many more discrete discharges are shown than indicated with arrows). (a) Weak continuous RF activity and frequent discrete discharges recorded on 17 April 2010 from 00:20 to 00:30 UTC. (b) Strong continuous RF activity and numerous discrete discharges recorded on 17 April 2010 from 04:30 to 04:40 UTC. (c) Intermittent continuous RF activity and numerous discrete discharges recorded on 17 April 2010 from 15:20 to 15:30 UTC. Colors indicate density of events, red being most events and purple least.

In addition to variations in intensity, continuous RF often occurred intermittently, as was observed from 15:20 to 15:30 UTC on 17 April, shown in Figure 3c. The intermittent occurrence of continuous RF throughout the entire first explosive period was likely the result of the eruptive activity being episodic, but it could also have been an indication that the charging on the volcanic ejecta was not always strong enough to produce continuous RF.

The first explosive period (14–18 April) was distinguished by vigorous eruptive activity, high wind speeds, and variable plume heights. As described in section 4, 35% of the total volume of erupted magma was produced during the first explosive period [*Gudmundsson et al.*, 2012]. During this period, the average plume height varied between 2.7 and 8.5 km, as shown in Figure 2b. The large standard deviations of the average plume height show that there was also significant variation in the 5 min radar data. Wind speeds, shown in Figure 2c, were very high throughout most of the first explosive period; the highest wind speeds observed during the entire eruption occurred between 15 and 17 April, ranging from approximately 25 m s^{-1} at 3 km altitude to 55 m s^{-1} at 7 km altitude.

Some of the variability in the plume height data is likely due to poor radar resolution and changes in the magma discharge rate, but changing wind speeds would also have been responsible for height variability. High wind speeds will affect the plume height of low mass eruptions, such as the 2010 eruption of Eyjafjallajökull, due to the entrainment of additional air into the plume and by shearing the vertical trajectory of the plume. *Woodhouse et al.* [2013] demonstrated that for a plume in a windy environment (wind speed of 30 m s^{-1}) to rise to the same height as a plume in a quiescent environment, the source mass flux would need to be approximately 1 order of magnitude higher than that of the quiescent environment [see

Woodhouse et al., 2013, Figure 3]. For example, the peak average plume height on 17 April was several kilometers higher than that on 16 April, and the average wind speed on 17 April was approximately 20 m s^{-1} lower than that on 16 April. Thus, though plume rise height is related to the source mass flux of an eruption [*Morton et al.*, 1956], the elevated plume heights on 17 April are not necessarily indicative of a more vigorous eruption and could have resulted, at least partially, from the reduction in wind speed.

Following the decline of major explosive activity on 18 April, lightning was detected infrequently during the effusive phase (18 April–5 May). During this 18 day period, a total of 38 discharges were detected by the LMA. Two-station correlations showed that nine of these discharges occurred during a short 7 h time interval between 19:00 UTC on 28 April and 01:40 UTC on 29 April, shown by the dotted line Figure 2a. The number of correlated sources for each discharge ranged from 100 to 1000. ATDnet detected four of these discharges. Additionally, the three-dimensional data showed that 17 small and 12 regular discharges occurred over the 22 h interval between 13:00 UTC on 3 May and 11:00 UTC on 4 May, shown as red and black lines in Figure 2a. None of these discharges were detected by ATDnet. The average plume height was commonly lower than 3 km during the effusive phase, however, both of these periods of intermittent lightning activity corresponded to an increase in the plume height, shown by comparing Figures 2a and 2b on 28–29 April and 3–4 May.

The second explosive period and the declining phase of activity (5–22 May) can be divided into two intervals—an initial interval where lightning occurred infrequently and a subsequent interval where lightning occurred frequently, as seen in Figure 2a. The first interval, when lightning was observed infrequently, occurred from 5 to 10 May. The second interval, when relatively high rates of lightning were observed, occurred between 11 and 21 May. This distinction was also observed by *Bennett et al.* [2010] and *Arason et al.* [2011c] in the ATDnet data.

During the interval when low lightning rates ($<$ 10 discharges per hour intermittently) were observed (5–10 May), average plume heights were also relatively low, and the ambient atmospheric temperatures were relatively high, as shown in Figure 2b. Between 5 and 8 May, average plume heights of 5 km with low standard deviation were typical, except for a brief deviation to 8 km at the end of 5 May. From 8 to 10 May the average plume height was still low but variable, ranging from 3 to 5 km. Throughout this entire period (5–10 May), the plume top was almost always warmer than −20°C. Additionally, wind speeds were high, ranging from 10–20 m s^{-1} at 3 km altitude up to 40 m s^{-1} at 7 km altitude, shown in Figure 2c.

During the relatively high-rate lightning interval (11–21 May), a wide range of lightning rates was observed. Rates of regular discharges ranged from $\sim$ 10 to $\sim$ 50 per hour, and rates of small discharges ranged from $\sim$ 10 to $\sim$ 150 per hour. By contrast, the peak lightning rate detected by ATDnet during the second explosive period was 15 discharges per hour, less than the peak LMA-detected rates of $\sim$ 50 per hour. ATDnet located a total of 790 discharges throughout the entire eruption, while the LMA detected approximately 7700 discharges from 1 to 22 May. This difference in detection rates between ATDnet and the LMA is expected due to the fundamental differences between the two systems, but ATDnet performed well in detecting the electrical activity.

Though they are considered high for the eruption of Eyjafjallajökull, the peak flash rates detected from 11 to 22 May were relatively low compared to the 2009 eruption of Redoubt Volcano. During the Redoubt eruption, the LMA-detected peak flash rates of regular discharges were on the order of 100 per minute [*Behnke et al.*, 2013], compared to roughly 1 per minute for Eyjafjallajökull. This is not surprising considering that Redoubt's largest eruptive events produced plumed heights up to 19 km, whereas the peak 1 h average plume height from Eyjafjallajökull was 8 km.

During the interval when relatively high lightning rates were observed, the average plume height varied significantly, and the ambient temperatures were lower than during the low-rate lightning interval, as shown in Figure 2b. At the onset of lightning on 11 May, the average plume height was approximately 5 km, similar to the 5–10 May period when little lightning was observed. On 13 May, the plume height increased significantly; from the end of 13 May to 17 May, the average plume height frequently reached up to 8 km. At the end of 17 May, plume heights declined and remained below 6 km for the remainder of the eruption. From approximately 13 to 18 May, the plume top was consistently colder than −20°C and was often colder than −30°C. At these temperatures, plume-based ice-contact charging would be expected to occur if ice particles were to form in the plume.

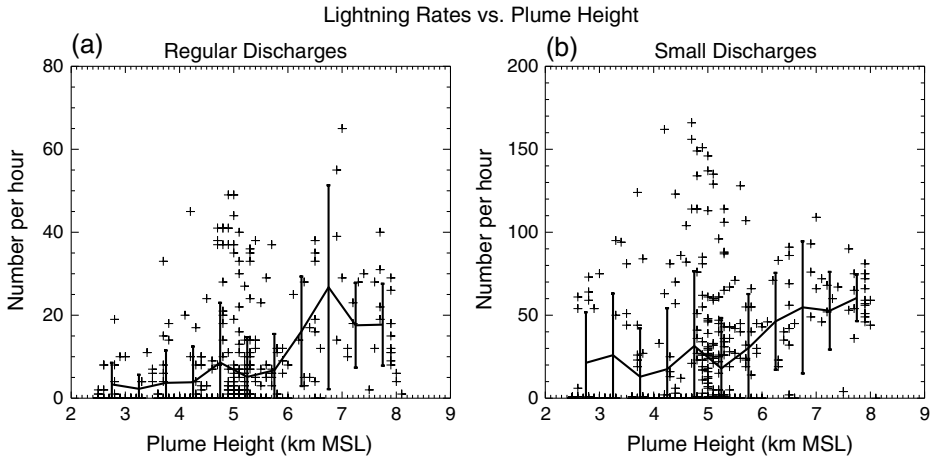

Figure 4. Scatter plot of the rate of (a) regular discharges and (b) small discharges per hour versus average plume height. In both plots, the black line shows the rates averaged over half kilometer plume height bins (2.0–2.5, 2.5–3.0, 3.0–3.5, etc.), showing an increase in average lightning rate with increasing plume height. Vertical bars show the standard deviation.

In addition to the variation in plume height, there was also a significant variation in wind speed from 11 to 21 May, shown in Figure 2c, which would have influenced the plume height. Wind speeds were high at the onset of lightning on 11 May, just as they were from 5 to 10 May when very little lightning was observed and plume heights of 5 km were typical. From 13 to 17 May, when plume heights up to 8 km were observed, wind speeds were much lower than they were from 5 to 10 May. The subsequent decrease in plume height on 17 May coincided with an increase in wind speed. As discussed earlier in this section, changes in wind speed are expected to be anticorrelated with changes in plume height; in this case the decreasing wind speeds on 13 May could have resulted in increasing plume height, and the decrease in the average plume height on 17 May could have been caused in part by the increase in wind speed.

The relationship between plume height and lightning during the second explosive period is shown Figure 4. Overall, there was a weak positive correlation between plume height and rates of both small and regular discharges. The black lines in Figure 4 show the lightning rates when averaged over half kilometer plume height bins, which shows that there was an increase in the average lightning rate with increasing plume height for both small and regular discharges. The increase in average lightning rate was most significant when the plume height was above 5 km (msl); however, the standard deviation of the average rates shows that there was a large variation in the observed lightning rates. Above altitudes of 5 km rates of regular discharges ranged from 0 to 65 discharges per hour, and rates of small discharges ranged from 0 to 130 discharges per hour. In addition, there was also a lot of variation at lower altitudes, particularly for small discharges. Below 5 km, the rate of small discharges varied between 0 and 100 discharges per hour. Overall, this plot shows that elevated plume heights did not always result in high lightning rates, and relatively high lightning rates occurred over a wide range of plume height. *Bennett et al.* [2010] compared plume height to ATDnet-detected lightning rates and also found that though lightning rate generally increased with plume altitude, there were many instances when elevated plumes did not produce lightning.

A correlation between plume height and lightning rates is difficult to interpret because it can be attributed to either plume-based ice-contact charging or vent charging mechanisms. For both mechanisms, an increase in plume height can affect charging or be indicative of increased charging. In the case of vent charging, an increase in plume height is indicative of an increase in source flux [*Morton et al.*, 1956]; thus, higher quantities of ash should correspond to an increase in charge in the plume. For the plume-based mechanism, increased plume height would contribute to an increase in ice-contact charging because the plume would be penetrating into lower atmospheric temperatures. The interpretation is further complicated by the effect that changing wind speed has on plume height, as described above.

Unlike the first explosive period, no continuous RF was observed during the effusive phase, the second explosive period, or the declining phase of explosive activity. The unprocessed data files were visually inspected, showing no obvious indications of continuous RF throughout these periods. Likewise, there were no correlated continuous RF events in the processed data. In the Redoubt Volcano data, correlated

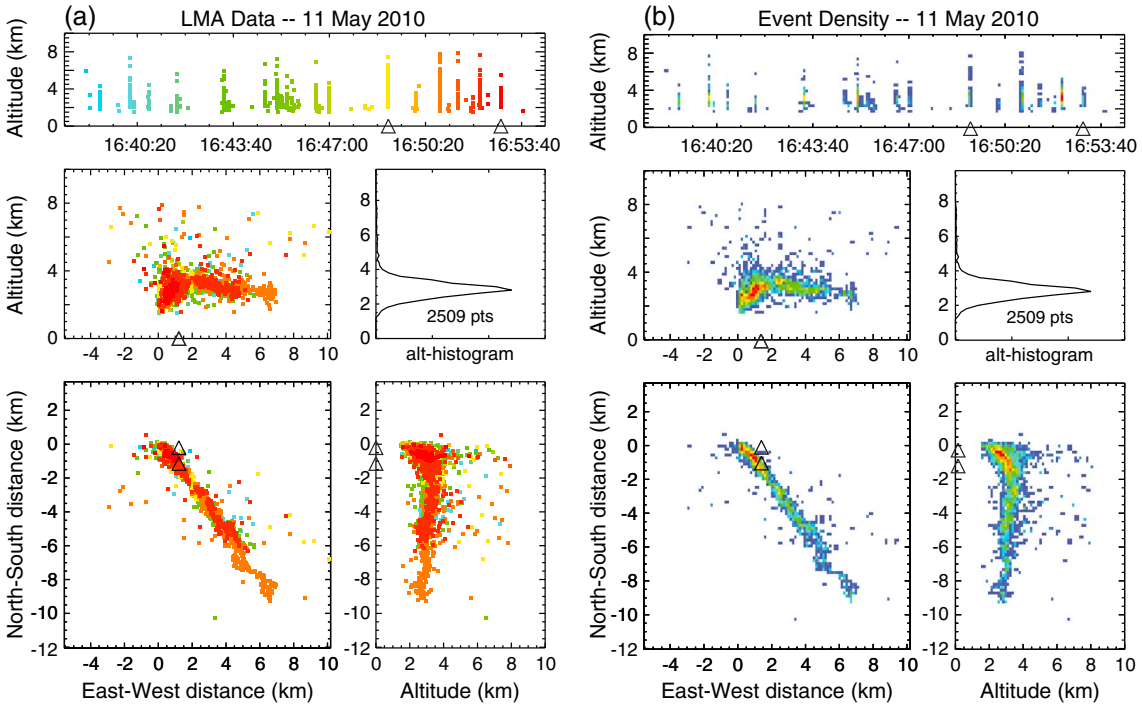

Figure 5. Fifteen minutes of processed LMA data from 16:39 to 16:54 UTC on 11 May 2010 colored by (a) time and (b) event density. Event density color scale is qualitative, red being most events and blue least. During this time, discharges commonly extended from the vent (located at the approximate coordinates (0, 0)) to the southeast. ATDnet detected two discharges during this period, indicated by the black triangles in Figures 5a and 5b. The event density (Figure 5b) shows the highest concentration of VHF sources located near the vent. In both Figures 5a and 5b, the top plot shows the altitude of the sources versus time, the middle left plot shows the altitude of the sources versus east-west position, the middle right plot shows an altitude histogram of the sources, the bottom left plot shows the plan position locations of the sources, and the bottom right plot shows the altitude of the sources versus north-south position.

continuous RF events manifested as swarms of VHF sources within a small distance over the vent of the volcano [*Behnke et al.*, 2013], but this was not observed in the Eyjafjallajökull data. Single-sources and two-source pairs were discarded from the Eyjafjallajökull data in the flash sorting process; however, these sources were unlikely to be from continuous RF. The continuous RF sources in the processed Redoubt data occurred so frequently that the XLMA flash algorithm had to be modified to avoid clumping these sources into amorphous, multisecond long discharges. There were no such issues with the Eyjafjallajökull data.

The lack of continuous RF during the second explosive period was unexpected since moderate amounts of lightning were observed during this period. The lack of continuous RF suggests that there was a reduction in the amount of vent charging compared to the first explosive period. One difference between the two explosive periods is that unlike the first period, the second explosive period was not phreatomagmatic. Thus, there would have been no charging due to boiling of water as there likely would have been during the first explosive period. This could account for the lack of continuous RF during the second explosive period. However, boiling of water is not necessary for continuous RF to occur. During the 2006 Augustine Volcano eruption, continuous RF was observed frequently, and that volcano did not have any significant snow or ice cover to cause substantial phreatomagmatic activity.

5.2. Three-Dimensional Lightning Mapping Observations

An example of processed, three-dimensional data from the second explosive period is shown in Figure 5. This figure shows 15 min of data on 11 May from 16:39 to 16:54, which was about 5 h after the onset of the relatively high-rate lightning period discussed above. During this 15 min interval, there were 19 regular discharges and 14 small discharges, corresponding to an average rate of roughly 1 discharge per minute (60 per hour) for both small and regular discharges. ATDnet detected two of the regular discharges, as indicated by the black triangles in Figure 5. The discharges extended from the vent of the volcano to the southeast during this period due to the upper level winds. The plume height was approximately 5 km at this time, and VHF sources extended from 2 to 5 km over the vent and from 2 to 4 km in the downwind plume. The altitude at the top of the vent is approximately 1.67 km. Figure 5b shows the density of located events,

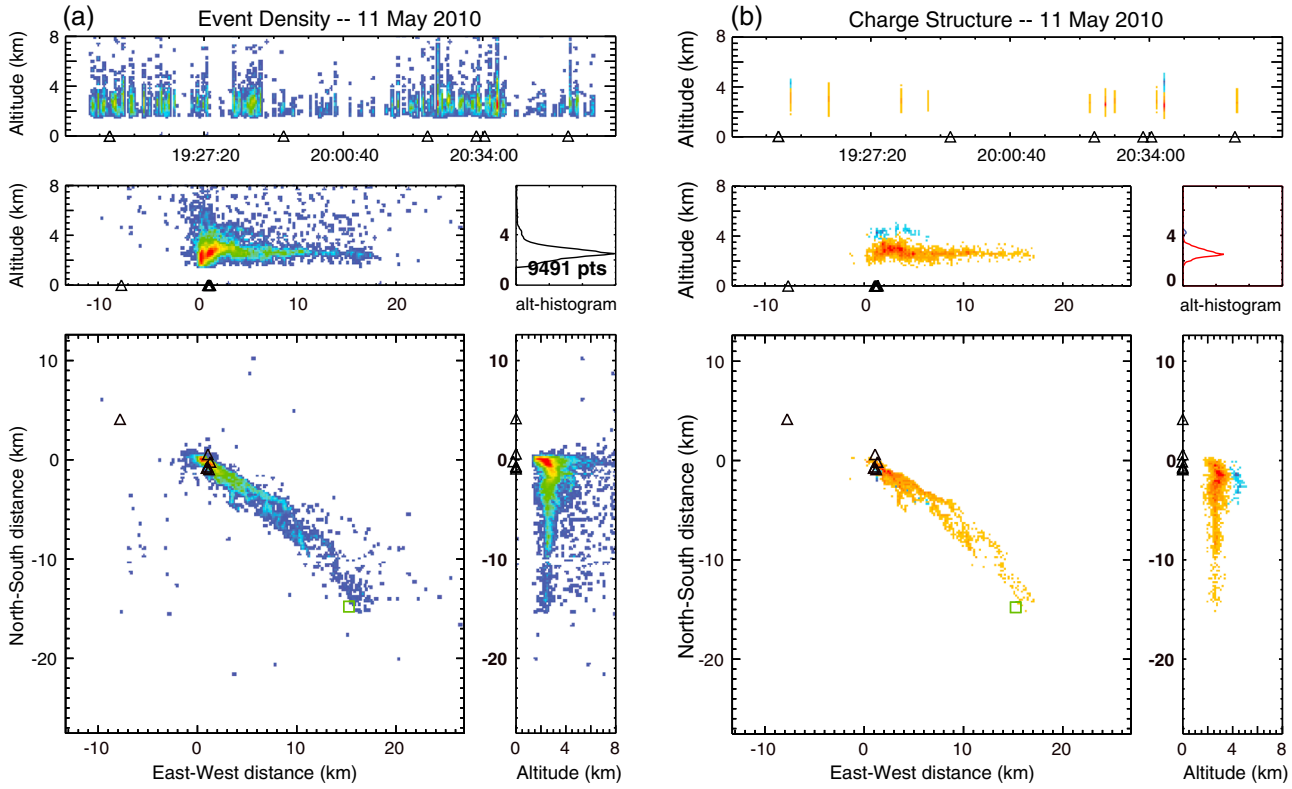

Figure 6. Two hours of electrical activity during a period of high winds. (a) Total LMA data from 19:00 to 21:00 UTC on 11 May 2010, colored by event density. Event density color scale is qualitative, red being most events and blue least. (b) Charge analyses of the larger discharges in Figure 6a, showing a dipolar charge structure consisting of positive charge centered at 2.5–3.0 km altitude and negative charge at 4 km altitude. Colors indicate charge density; orange is positive charge density, and blue is negative charge density. The vent altitude is 1.67 km. The green square in the lower left plot of Figures 6a and 6b indicates the location of the "Snow" LMA station.

which reveals that the highest density of sources was located between 2 and 4 km altitude and within 2 km horizontally of the vent. The importance of high densities of VHF sources near to the vent will be discussed in more detail in section 5.2.5.

Individual discharges such as those from Figure 5 were examined using the charge analysis method described in section 2.1.1. The charge analysis method was performed only on the discharges that exhibited obvious channel structure, and discharges were chosen manually. Only about 10% of the regular discharges from the entire second explosive period were suitable for the analyses, and no small discharges were used. There were several extended periods of time when the charge analysis method could not be used due to the compact size of the discharges.

The charge structure in the plume varied between an apparent positive monopole and a negative-over-positive dipole throughout the second explosive period. The time periods during which charge structures could be identified are indicated in Figure 2a by the shaded pink (monopole structure) and blue (dipole structure) bars. The periods when no lightning occurred and when the charge structure was indeterminable remain white. The positive monopole was more common than the dipole. Dipolar structures were generally inferred only for brief periods of time. The results do not preclude the existence of other regions of charge in either the dipole or monopole case; they simply show the charge regions where electrical breakdown was detected.

Four examples of the inferred charge structures are presented below. Each example represents a period when high rates of regular discharges were observed during the second explosive period and are presented in chronological order. The first three examples show evidence of a dipolar electrical structure, and the fourth example shows the more common monopolar structure.

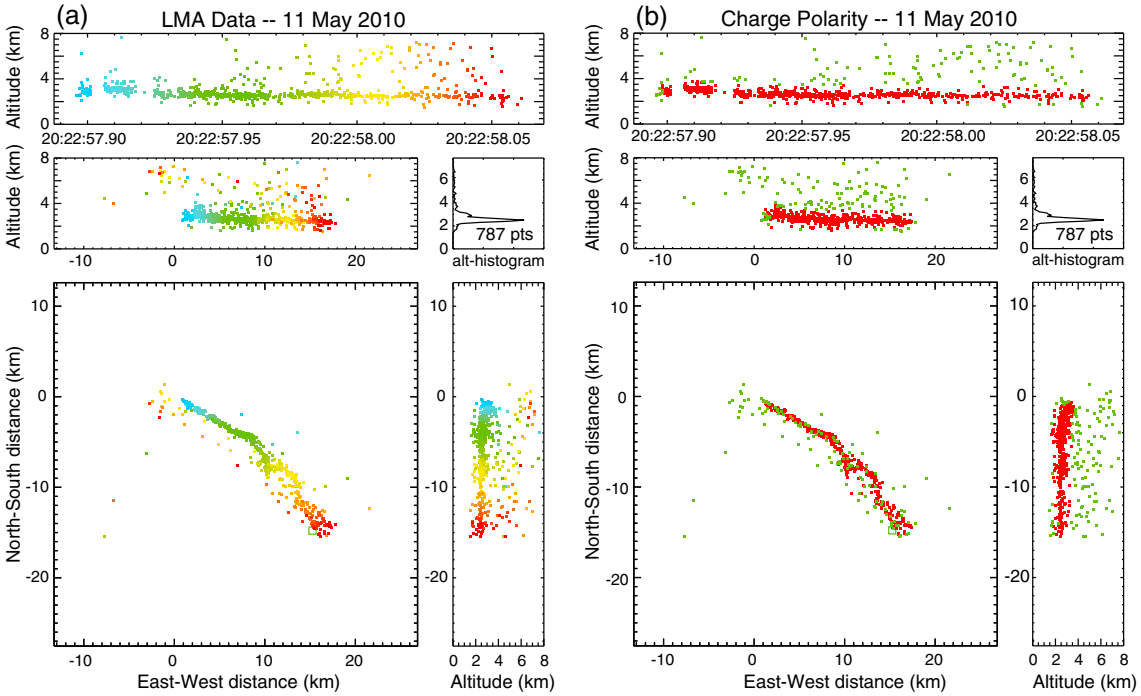

Figure 7. (a) LMA data for a long discharge on 11 May 2010 at 20:22:57.9 UTC extending from the vent of Eyjafjallajökull to the southeast, colored by time. (b) Same as Figure 7a, but colored by charge polarity. Red indicates regions of positive charge, and green indicates undetermined charge polarity. This discharge showed evidence only of negative polarity breakdown into a region of positive charge.

5.2.1. 11 May 19:00–21:00 UTC

About 8 h after the onset of high rate electrical activity during the second explosive period, a negative-over-positive dipolar charge structure was inferred on 11 May from 19:00 to 21:00 UTC, shown in Figure 6. Over this 2 h period, the charge structure consisted of a horizontally elongated positive charge region extending from the vent of the volcano approximately 23 km to the southeast, indicated by the orange region in Figure 6b, and a negative charge region located above the positive region with a length of approximately 8 km, indicated by the blue region in Figure 6b. The positive region had a depth of 2 km and was situated between 2 and 4 km altitude. The negative region was located between approximately 4 and 5 km altitude. Flash rates were approximately 50 and 70 discharges per hour for regular and small discharges, respectively. In comparison, ATDnet detected a total of six discharges during this 2 h period. Figure 6a shows the event density for 19:00–21:00 UTC. The event density was highest near the vent of the volcano, in the lower positive charge region. The elongated shape of the charge structure was likely due to high winds advecting charge into the downwind plume. Winds were northwesterly with speeds ranging from approximately 15 m s^{-1} at 3 km altitude to 35 m s^{-1} at 7 km altitude. The average plume height was 5 km.

The individual lightning discharges observed during this time period were typically long and thin, extending up to 23 km from the vent, presumably being confined within the plume. Of the 10 discharges selected for charge analysis during this period, two discharges showed evidence of both positive and negative polarity breakdown and eight showed evidence of negative polarity breakdown only. It is not clear if the discharges that showed evidence only of negative polarity breakdown were truly monopolar, initiating from ground, for example, and extending up and into the downwind plume, or if they were bilevel intracloud discharges whose positive ends were simply undetected.

An example of one of the discharges that showed evidence only of negative polarity breakdown into positive charge is shown in Figure 7. This example shows a negative polarity leader extending from the vent to approximately 23 km to the southeast. The discharge occurred on 11 May at 20:22:57 UTC. Figure 7a shows the VHF sources colored by time, and Figure 7b shows the VHF sources colored by the inferred charge. In this and other figures of individual discharges showing charge identification, color is used to convey the polarity of the charge region into which the breakdown propagated. Red indicates negative breakdown into positive charge, blue indicates positive breakdown into negative charge, and green indicates that the charge region

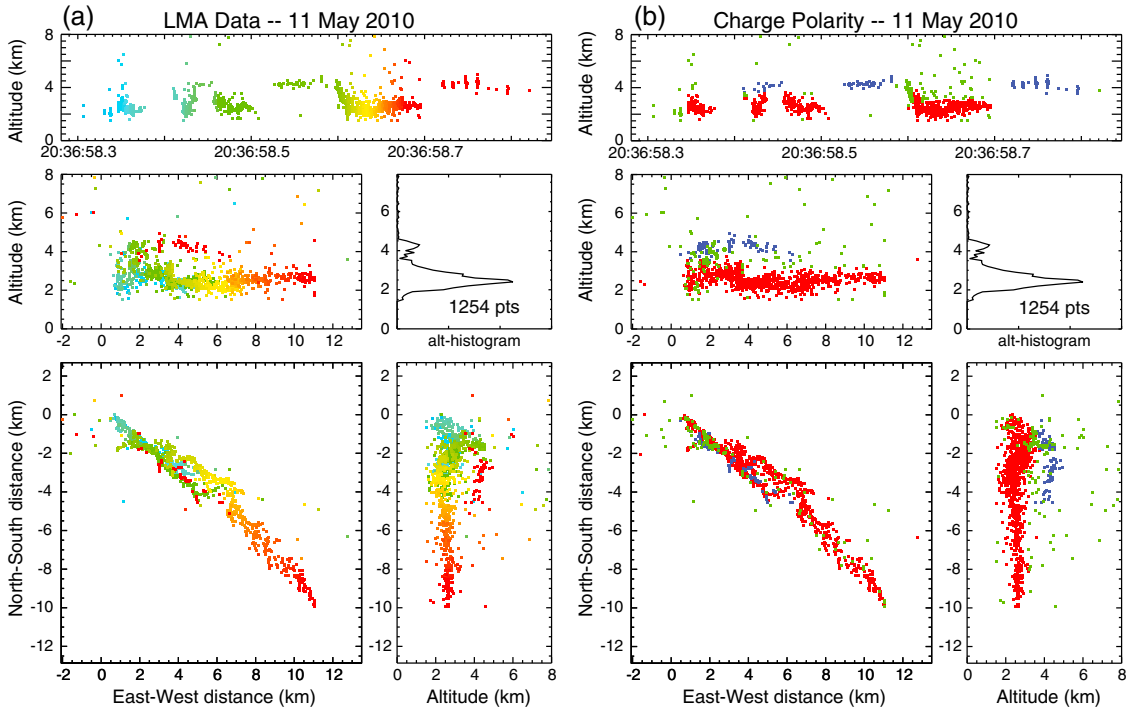

Figure 8. (a) LMA data for a bilevel discharge on 11 May 2010 at approximately 20:36:58.3 UTC extending from the vent of Eyjafjallajökull to the southeast, colored by time. (b) Same as Figure 8a, but colored by charge polarity. Red indicates regions of positive charge, blue indicates regions of negative charge, and green indicates undetermined charge polarity. This flash showed clear evidence of both negative breakdown into positive charge and positive breakdown into negative charge.

was either undetermined or that the sources were noise or noise-affected solutions. In this case, there was no indication of positive polarity breakdown into negative charge. The first several VHF sources in this discharge were located at 2.5 km altitude, approximately 800 m above and 1 km downwind of the vent. This discharge may have initiated at the ground near the vent of the volcano and propagated up as negative polarity breakdown into positive charge in the downwind plume. In this case there would have been only one polarity of breakdown to detect and the flash's upward development would not have produced a high current return stroke, consistent with it not being detected by ATDnet. It is also possible that the discharge initiated above ground, and the positive breakdown was not detected by the LMA.

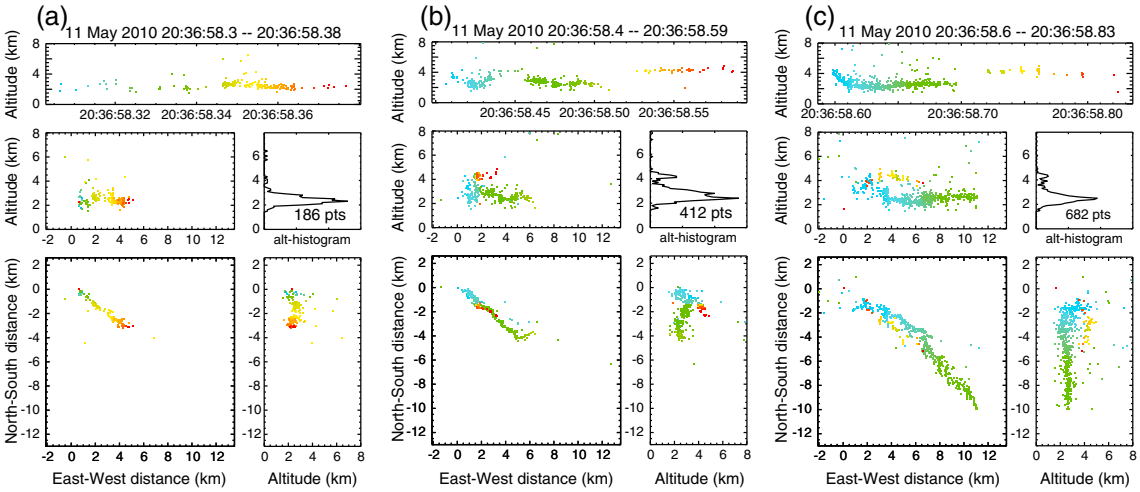

Figure 9. Flash from Figure 8 broken into three shorter time intervals to show the flash's three overlapping and extending channels, colored by time. (a) First channel, occurring between approximately 20:36:58.3 and 20:36:58.38. (b) Second channel, occurring between approximately 20:36:58.4 and 20:36:58.59. (c) Third channel, occurring between approximately 20:36:58.6 and 20:36:58.83. Such bilevel breakdown is typical of thunderstorms, but this discharge initially began at low altitude above the vent and transitioned into a bilevel discharge (see text).

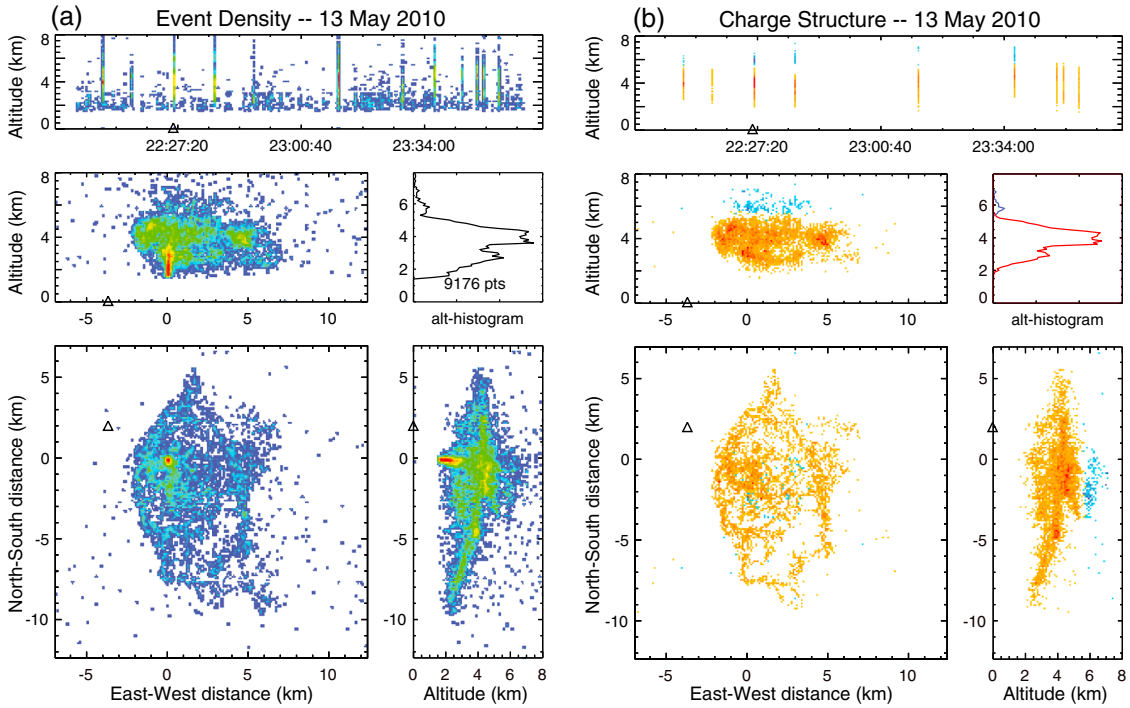

Figure 10. Two hours of electrical activity during a period of relatively low winds. (a) Total LMA data from 22:00 to 23:59 UTC on 13 May 2010, colored by event density. (b) Charge analyses of the larger discharges in Figure 10a, showing a negative-over-positive dipolar charge structure. Colors indicate charge density; orange is positive charge density, and blue is negative charge density.

An example of a discharge that showed evidence of both negative polarity breakdown into positive charge and positive polarity breakdown into negative charge is shown in Figure 8. This discharge occurred on 11 May 2010 at 20:36:58.3 UTC. Unlike the previous example shown in Figure 7, the structure of this discharge resembles an intracloud discharge occurring in a low-altitude positive charge region and negative charge region located above the positive. The positive and negative ends of the leader were readily distinguishable, shown as the blue and red sources in Figure 8b. An interesting feature of this discharge is that it propagated in repeated spurts, retracing a similar path each time.

Figure 9 shows the discharge of Figure 8 broken into three separate time intervals, showing that the discharge initiated at low altitude and transitioned into a bilevel flash. The initial negative polarity breakdown, shown in Figure 9a, propagated from $(x, y) \simeq (0.5, 0.0)$ to $(5.0, -3.0)$ km. The discharge appeared to initiate at low altitude (approximately 2 km). After a lull of approximately 30 ms, negative polarity breakdown resumed, again starting at $(0.5, 0.0)$ and propagating slightly farther to $(6.0, -4.0)$, following a very similar path, but starting higher in altitude at approximately 3.5 km. During this second period, shown in Figure 9b, positive breakdown into negative charge was also inferred, shown as the blue sources between 20:36:58.4 and 20:36:58.52 at 4 km altitude in Figure 8. At approximately 20:36:58.6, negative polarity breakdown recommenced, this time at $(0.5, -1.5)$ and 4 km altitude, as shown in Figure 9c. The breakdown began about 1.5 km south of the other two segments and extended farther to the southeast along a similar path as the others. Subsequently, positive breakdown into negative charge was inferred again at 4 km altitude, shown in Figure 9c.

5.2.2. 13 May 22:00–23:59 UTC

At the end of 13 May, the average plume height had increased from 5 to 8 km, which coincided with a decrease in wind speed, as shown in Figures 2b and 2c. Prior to the increase in plume height, the inferred charge structure was predominantly monopolar, but following the increase, a negative-over-positive dipolar structure was inferred between 22:00 and 23:59 UTC on 13 May, as shown in Figure 10. Unlike the previous example from 11 May, shown in Figure 6, the charge structure was not elongated, likely due to the lower wind speeds, which had calmed to nearly 0 m s^{-1} at the 3 and 5 km levels and 5 m s^{-1} at 7 km altitude level by this point in the eruption. In addition, a somewhat higher percentage of the discharges in this example showed evidence of bipolar breakdown than in the previous example. Out of nine discharges selected for

charge analysis during this period, four showed evidence of bipolar breakdown and five showed evidence only of negative breakdown into positive charge. As shown in Figure 10, the structure consisted of a large positive charge region between 2 and 5 km altitude and a negative charge region between 5.5 and 7.0 km altitude. Similar to the previous example, the highest density of events was located low in altitude and near to the vent, as shown in Figure 10a. Flash rates during this 2 h period were lower than the previous example; approximately 15 discharges per hour were detected for regular discharges and 60 discharges per hour were detected for small discharges. Only one discharge was detected by ATDnet during this period.

An example of one of the bipolar discharges is shown in Figure 11. This discharge occurred at 22:28:08.4 UTC on 13 May. The discharge is different from the previous examples because it was also detected by ATDnet, as indicated by the black triangles in Figures 11a–11c. Detection by ATDnet suggests that the discharge was a cloud-to-ground flash. To better illustrate the morphology of the discharge, it has been divided into two intervals, labeled "part 1" and "part 2" in Figure 11a. The first part of the discharge is shown colored by source power in Figure 11c. This part of the discharge originated at 2 km altitude directly over the vent and propagated up to 4 km altitude. The ATDnet detection then occurred, which was followed by subsequent breakdown to the south-southeast at 3 km altitude. The polarity of the first part of the discharge is uncertain and is thus colored green in Figure 11b. The relatively strong source powers shown in Figure 11c suggest that the first part was negative polarity breakdown into positive charge. If it was indeed negative polarity breakdown, and if what ATDnet detected was a return stroke, it would follow that the cloud-to-ground discharge was positive (i.e., it lowered positive charge to ground). The second part of the discharge, shown colored by source power in Figure 11d, involved negative breakdown between approximately 2 and 5 km altitude and positive breakdown at 6 km altitude. The negative breakdown propagated in a circular fashion, perhaps delineating the edge of the plume. Such circularity is not seen in meteorological storms. The entire flash is shown colored by inferred charge polarity in Figure 11b. Though the polarity of the first part of the flash may be uncertain, it is very clear that there was breakdown into an upper region of negative charge and a lower region of positive charge during part 2 of the flash. Without more certain knowledge of the return stroke polarity, it is difficult to offer any further interpretation of this discharge. The discharge was complex and suggests that the charge structure was more complicated than a simple dipole, but without better data, the finer structure remains unknown.

During the 2 h time period of Figure 10 and the succeeding 2 h time period of 00:00–02:00 on 14 May, several other discharges occurred that exhibited a similar morphology, beginning with a presumed positive cloud-to-ground discharge followed by a low-altitude intracloud component. The discharges are not fully understood but may be some sort of hybrid cloud-to-ground/intracloud discharge. Regardless, this time period showed the most consistent evidence of a dipolar structure of the entire eruption. This is probably due to the low and unvarying wind speeds at the time and perhaps indicates that the eruption was in a more or less steady state.

5.2.3. 16 May 14:00–16:00 UTC

On 16 May, wind speeds were again relatively low and the average plume height reached up to 8 km, similar to the conditions of the 13 May example discussed above, except there was more variability in the plume height. As shown in Figure 2b, the average plume height on 16 May from 14:00 to 16:00 UTC varied between 6.5 and 8 km. During the 14:00–16:00 UTC period, winds were northwesterly with speeds ranging from 5 m s^{-1} or less at 3 km altitude to 10 m s^{-1} at 7 km altitude.

Throughout 16 May, the inferred charge structure was predominately monopolar; however, dipolar structures were also inferred for brief periods of time. One of these brief dipolar periods occurred during the 14:00–16:00 time period, which is shown in Figure 12. Twenty discharges from this time period were suitable for charge analyses, only two of which showed evidence of bipolar breakdown. What is interesting about this example is that the polarity of the upper charge region between 4 and 6 km altitude changed with time. Between altitudes of 2 and 4 km, positive charge was consistently inferred throughout the entire period, but between 4 and 6 km, the inferred charge was initially negative and then changed to positive, as discussed in more detail below. As with the other charge structure examples, the greatest density of events was located near the vent and low in altitude, as seen in Figure 12a. During this 2 h period, flash rates were 40 and 90 discharges per hour for regular and small discharges, of which 19 were detected by ATDnet.

Figure 13 shows the LMA data from 14:00 to 16:00 broken into shorter intervals, illustrating the temporal variation of the polarity of the 4–6 km altitude region. From 14:00 to 14:30, the 4 to 6 km altitude region was

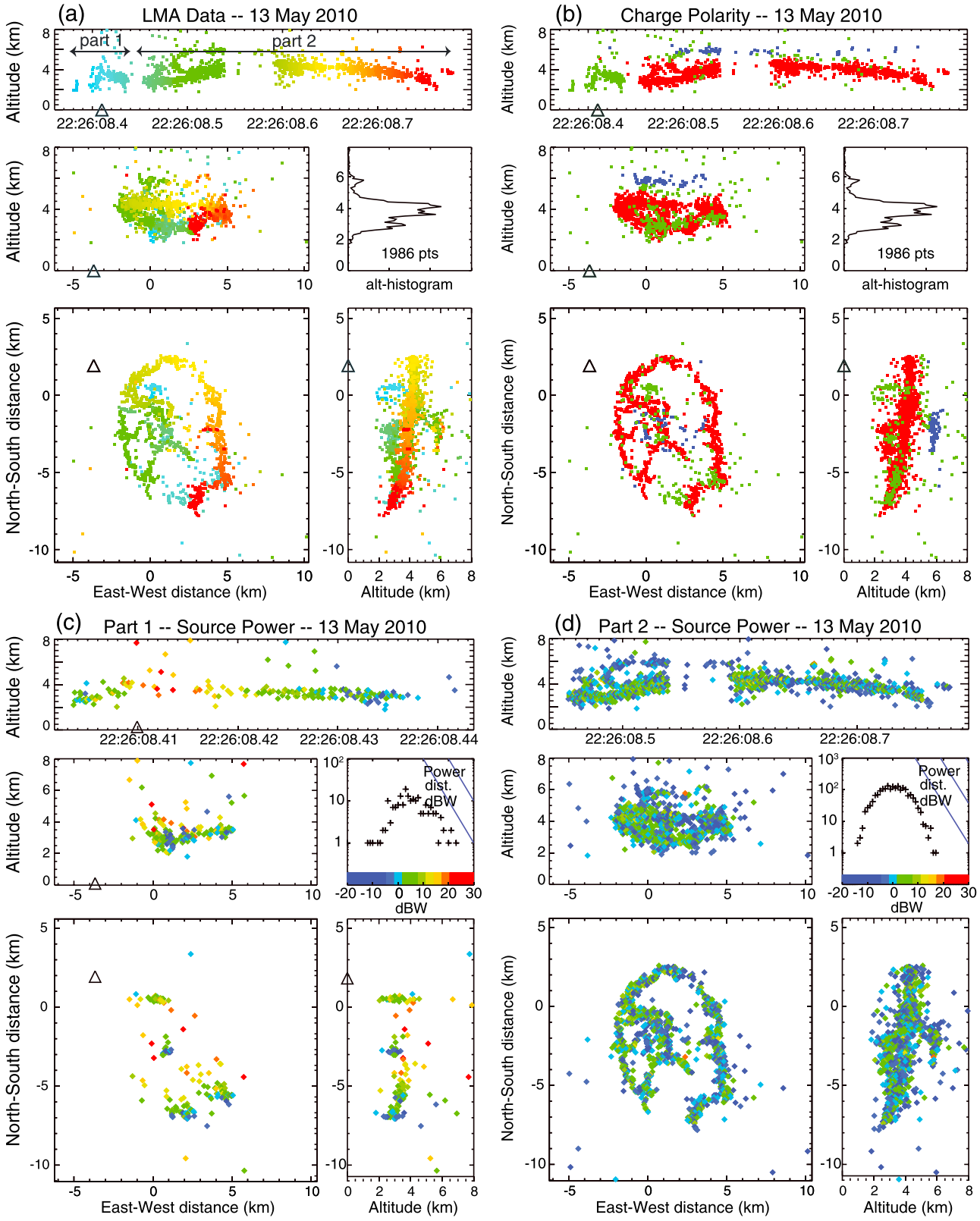

Figure 11. (a) LMA data for the bipolar discharge on 13 May 2010 at 22:28:08.4 UTC, colored by time. (b) Same as Figure 11a, but colored by charge polarity. Red indicates regions of positive charge, blue indicates regions of negative charge, and green indicates regions with undetermined charge polarity. (c) The part of the discharge shown in Figure 11a labeled as "part 1." (d) The part of the discharge shown in Figure 11a labeled as "part 2." The colors of the sources in Figures 11c and 11d indicate the amplitude of the source power. A histogram of the power distribution for Figures 11c and 11d is shown below and to the right of the upper time-height plot. The discharge was detected by ATDnet (black triangles).

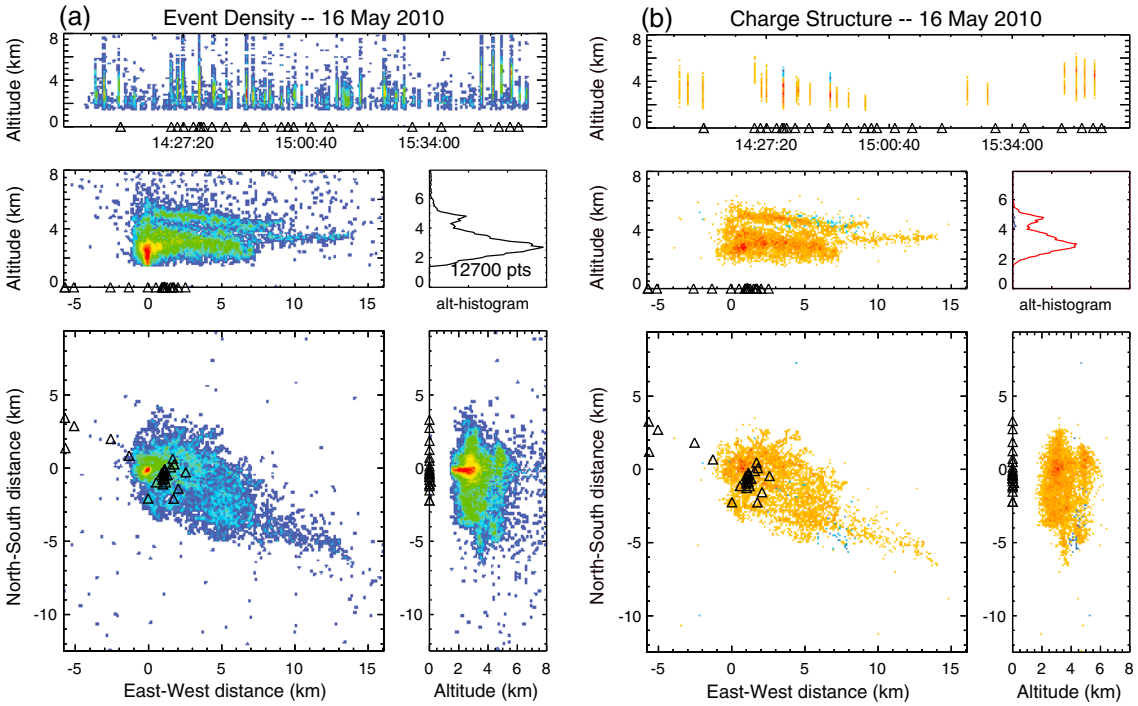

Figure 12. Electrical activity during a 2 h period on 16 May 2010. (a) Total LMA data from 14:00 to 16:00 UTC on 16 May 2010, colored by event density. (b) Charge analyses of the larger discharges in Figure 12a, showing a variation from a dipolar to monopolar charge structure. Colors indicate charge density; orange is positive charge density, and blue is negative charge density.

mostly devoid of electrical activity, except for a small region of positive charge approximately 1 km in diameter, centered over the vent (Figure 13d). Between 14:30 and 15:37, negative charged was briefly inferred between 4 and 6 km, extending 10 km southeast of the vent (Figure 13e). Between 15:37 and 16:00, positive charge was inferred between 4 and 6 km altitude, in the region where negative charge was inferred approximately 1 h earlier (Figure 13f). Note that for about 15 min leading up to the time when positive charge was inferred between 4 and 6 km (Figure 13c), there was no electrical activity in that region. The lull in upper level activity and the subsequent change in polarity of the upper charge region indicates some sort of variation with the charging mechanisms occurred that resulted in strong positive charge overriding the dipolar charge, possibly due to increased strength in the eruption that elevated the charge layers to the point that no positive breakdown occurred or was detected in the upper negative layer. As a result, the apparent monopolar structure inferred from 15:37 to 16:00 developed a bilevel distribution with respect to altitude, a feature that has also been inferred in the 17 May example, presented below. This particular bilevel distribution was not due to the discharges accessing one or the other of the lower and upper positive charge regions alone; each discharge observed in this period propagated into both layers.

5.2.4. 17 May 12:00–14:00 UTC

The final charge analysis example to be presented is of a positive monopolar structure inferred on 17 May from 12:00 to 14:00 UTC, shown in Figure 14. At this time, the average plume height was again approximately 8 km, but, similar to 16 May, there was a lot of variability in the altitude. Between 12:00 and 14:00 UTC, wind speeds were less than 10 m s^{-1} at the 3 and 5 km altitude levels and approximately 20 m s^{-1} at the 7 km level, with the speed at all levels increasing throughout the day. The wind direction also varied with altitude; at the 3 km altitude level, the wind was consistently easterly, but at the 5 and 7 km altitude levels, the wind direction briefly deviated between easterly and westerly. All 17 discharges for which charge analyses were made showed evidence only of negative polarity breakdown into positive charge. Figure 14a shows the event density of the radiation sources during this time period, which again shows that the highest density of events was located right over the vent at low altitude. Rates of regular and small discharges were 20 and 70 discharges per hour. ATDnet detected 17 discharges during this period.

The charge structure shown in Figure 14b is interesting because there were two distinct layers of positive charge, one of them being downwardly slanted in altitude with distance from the vent. Similar to the other

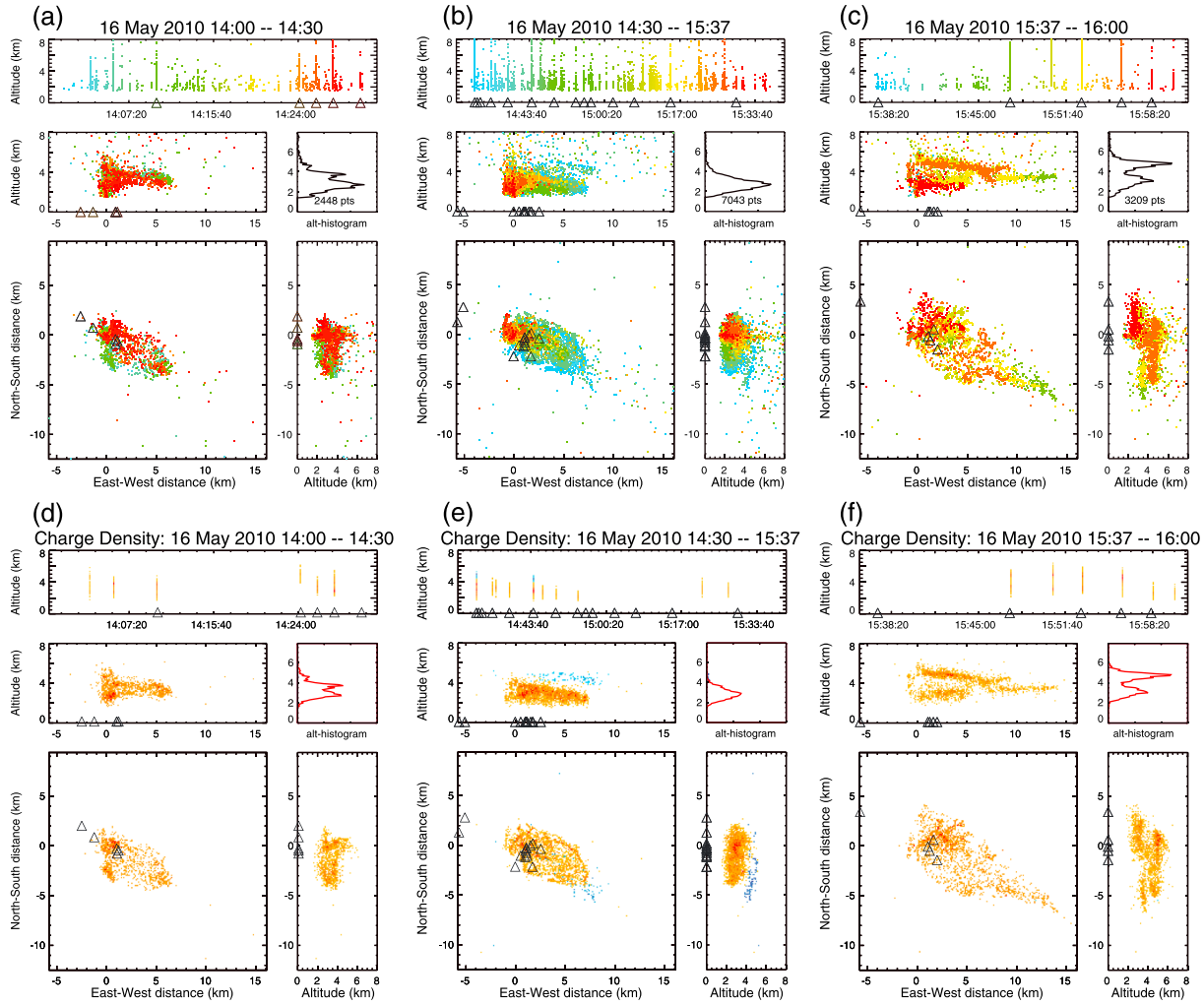

Figure 13. Data from Figure 12 broken into three shorter time intervals showing how the polarity of the upper charge region changed with time. LMA data colored by (a) time and (d) charge density for the period between 14:00 and 14:30 UTC on 16 May. LMA data colored by (b) time and (e) charge density for the period between 14:30 and 15:37 UTC on 16 May. LMA data colored by (c) time and (f) charge density for the period between 15:37 and 16:00 UTC on 16 May. Colors in Figures 13d–13f indicate charge density; orange is positive charge density, and blue is negative charge density.

charge structure examples, there was a lower layer of positive charge between 2 and 4 km altitude, which in this case extended from the vent to approximately 5 km east of the vent. In addition, there was also an upper layer of positive charge that was tilted down from west to east. The western edge of this layer was located over the vent and had a maximum altitude of 6 km, while the eastern edge extended out to 10 km from the vent where it had a minimum altitude of 2 km. Though there was evidence only of positive charge in this example, there may still have been an upper layer of negative charge like the other examples that simply did not have any electrical activity detected within it. The strange shape to the overall charge structure may be due to the changing wind conditions. As mentioned above, the wind direction at the 5 and 7 km altitude levels changed direction from easterly to westerly during this time period, while at the 3 km level the wind direction was consistently westerly. The easterly winds may have temporarily sheared the upper part of the plume toward the west and advected positive charge in that direction.

Many of the discharges observed between 12:00 and 14:00 UTC were similar to the example shown in Figure 15. This discharge, which occurred at 12:06:41.02 on 17 May, showed evidence only of negative polarity breakdown into positive charge. It initiated over the vent of the volcano at approximately 2 km altitude, first propagating horizontally to 4 km east of the vent, then up and into the slanted positive charge layer seen in Figure 14. The discharge produced two branches into the upper region of positive charge, one that propagated up and to the west and another that propagated down and to the east. Figure 15b shows

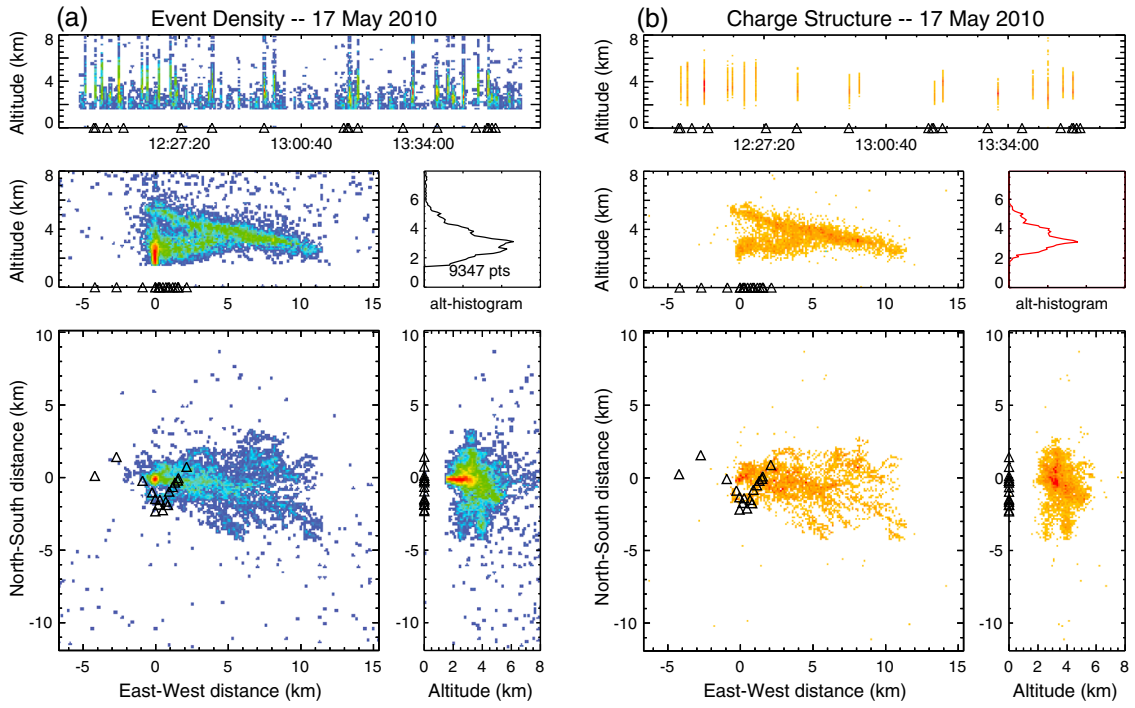

Figure 14. Electrical activity during a 2 h period on 17 May 2010. (a) Total LMA data from 12:00 to 14:00 UTC on 17 May 2010, colored by event density. (b) Charge analyses of the larger discharges in Figure 14a, showing a monopolar charge structure. Colors indicate charge density; orange is positive charge density, and blue is negative charge density.

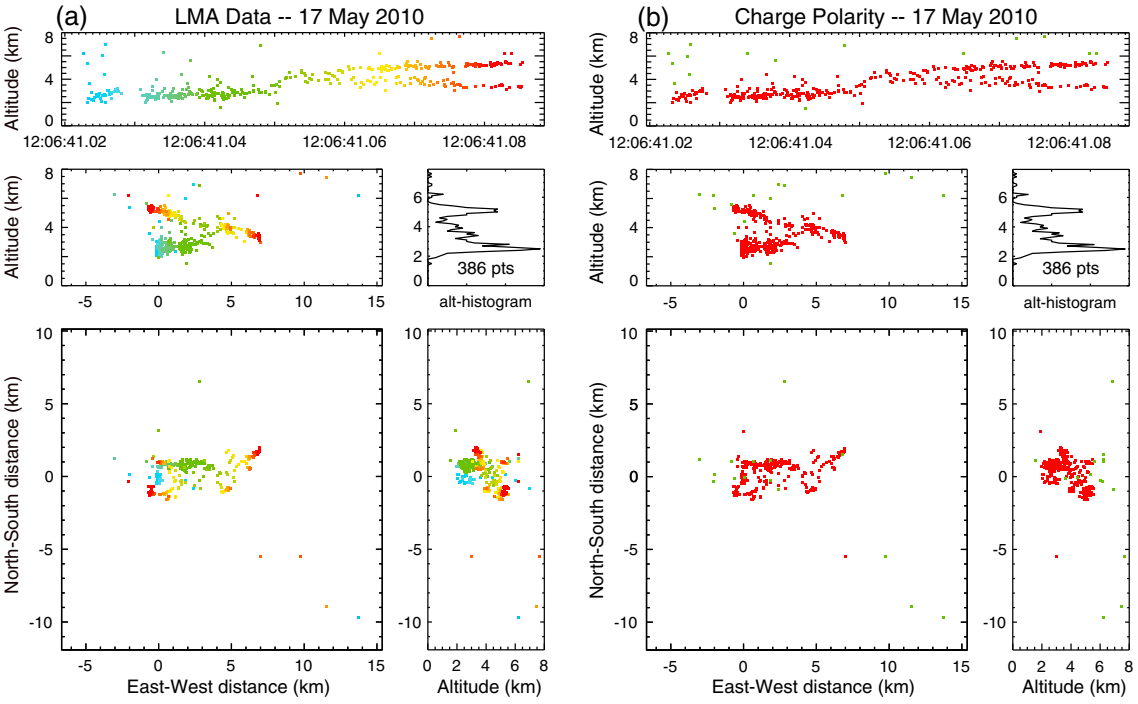

Figure 15. (a) LMA data for a monopolar discharge on 17 May at approximately 12:06:41 UTC, colored by time. (b) Same as Figure 15a, but colored by charge polarity. Red indicates regions of positive charge, and green indicates undetermined charge polarity.

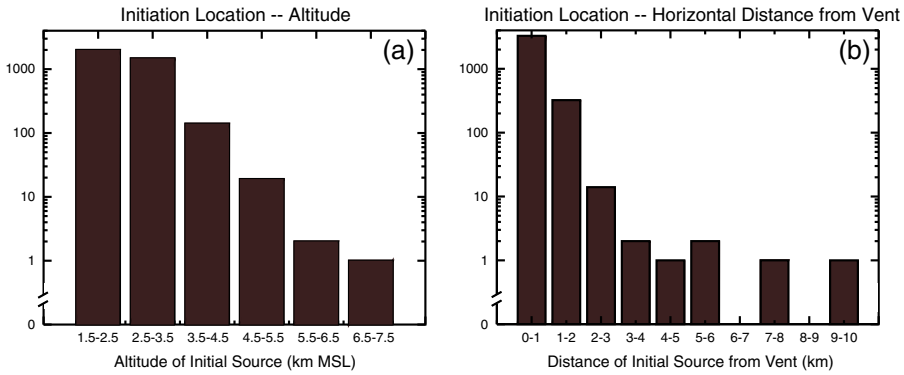

Figure 16. Lightning initiation locations of the three-dimensional data collected during May 2010. (a) Histogram of the average altitude of the first three VHF sources of each regular discharge. (b) Histogram of the average horizontal distance from the vent of the first three VHF sources of each regular discharge. Discharges typically initiated below altitudes of 4.5 km and within 2 km horizontally away from the vent.

charge identification results for the discharge, which was entirely due to negative polarity breakdown into positive charge. The other discharges that occurred during the 12:00 to 14:00 period followed very similar paths, though not all propagated bidirectionally in the slanted charge layer. At the beginning of the time period, the discharges propagated bidirectionally similar to the example shown in Figure 15, but toward the end of the time period, the discharges mainly propagated down and into the eastern region of the layer, perhaps due to the changes in wind speed and direction discussed above.

5.2.5. Location of High Densities of Electrical Activity

In each of the charge structure examples presented above, it was noted that the highest concentration of VHF sources was consistently located over the vent at low altitude. As shown in Figures 6a, 10a, 12a, and 14a, electrical activity was concentrated around the coordinates (0, 0) in east-west position and north-south position, corresponding to the approximate location of the vent of the volcano, and extended in altitude from 2 to 3 km. The altitude at the top of the vent is 1.67 km. The high concentration of VHF sources over the vent indicates that it was a region with very active, ongoing charging.

In addition to the high concentration of VHF sources being located over the volcano, regular discharges typically initiated in the same region, as documented by the histograms in Figure 16. The initiation points were determined by taking the average of the locations of the first three VHF sources for each discharge. Out of 3635 regular discharges detected during May, 55% initiated below 2.5 km altitude and 96% initiated below 3.5 km altitude. In terms of horizontal distance, 91% initiated within 1 km of the vent and 99% initiated within 2 km of the vent. For comparison, most of the lightning detected by ATDnet was located within 3 km of the vent, comparable to the uncertainty of the ATDnet data. In general, the uncertainty of the non-noise-contaminated LMA solutions was on the order of 20 m in horizontal position and 200 m in altitude, but if noise-contaminated solutions happened to be one or more of the first three sources of a discharge, then the error could be much greater. A noise solution of any altitude can be grouped with a discharge by the flash algorithm if it was within 3000 m horizontally and 150 ms of another source in a discharge, adding bias to the initiation altitude. Approximately one fourth of the discharges were inspected manually, and it was found that many noise solutions were often grouped with individual discharges by the flash algorithm, despite steps to limit the amount of noise in the post-processed data (Appendix A). Flashes with initiation altitude higher than 4.5 km were visually inspected, and in each case the high initiation altitude was due to the influence of high altitude noise solutions. Thus, most regular discharges initiated below 3.5 km altitude and all initiated below 4.5 km altitude. This roughly corresponds to the region where the highest densities of VHF sources were located (2–3 km altitude) and indicates further that the most active region of charging was near the vent at low altitude.

5.3. Charging Mechanisms

It is expected that both vent charging and subsequent plume-based charging can be involved in volcanic plume electrification and that the specific eruptive and meteorological conditions are important in determining how the mechanisms combine to produce the overall electrification. In the case of Eyjafjallajökull, the LMA data provide strong evidence that vent charging dominated, with most electrical activity occurring

near the vent. There is also some evidence that plume-based ice-contact charging may have occurred due to changing meteorological conditions, but the three-dimensional LMA observations do not indicate that ice-contact charging played a substantial role in plume electrification.

The evidence showing that vent charging was influencing the electrification comes from the examination of the three-dimensional lightning mapping data. The LMA data presented in section 5.2 show that the most electrically active region in the plume was located low in altitude and near the vent of Eyjafjallajökull. Figures 6a, 10a, 12a, and 14a show that the highest density of VHF sources was consistently located over the vent, between altitudes of 2 and 3 km and Figure 16 shows that lightning typically initiated in the same low-altitude, near-vent region. This electrically active region is so low in altitude that it would not have harbored the conditions necessary for plume-based ice-contact charging. Volcanic ejecta are initially very hot, on the order of 1000°C, but rapidly cool, reaching ambient temperature at the level of neutral buoyancy. Results from an integral plume model show that during the first explosive period, the plume was warmer than 0°C below altitudes of 4 km [*Woodhouse et al.*, 2013]. The model incorporates meteorological profiles of temperature, water vapor, and wind to predict plume height and trajectory based on volcanic source conditions including temperature, exit velocity, exit angle, gas fraction, vent radius, and vent altitude. Model results of the plume during the first explosive period showed that at 3 km the plume temperature was approximately 80°C, 90° warmer than ambient, and at 4 km the plume was approximately 10°C, 30° warmer than ambient. The ambient temperatures during the time period modeled by *Woodhouse et al.* [2013] were similar to the colder periods of the second explosive period. Thus, though the eruptive activity may have been different during the second explosive period, the modeled temperatures given by *Woodhouse et al.* [2013] give a reasonable estimate of the in-plume temperatures during the colder intervals of the second explosive period. Therefore, it is expected that the plume was too warm for ice to exist below altitudes of 4 km and that ice-contact charging could not have been directly electrifying this region. Further, it is not expected that charged particles separated at higher altitudes due to plume-based ice-contact charging would settle down to the near-vent region due to the dynamics of the eruption. Thus, that so much electrical activity was occurring so close to where volcanic ejecta were being erupted indicates that charged ejecta were electrifying this region.

The predominance of a low-altitude region of positive charge indicates that the ejecta carried a net positive charge as a result of vent charging mechanisms, leaving a net negative charge behind on the vent of the volcano. Both fracture charging and silicate contact charging likely contributed to this result, but it is not clear which mechanism was dominant. In the *James et al.* [2000] laboratory fracture charging experiments, negative charge was typically imparted on fractured silicate particles, though the most silica-poor sample ($\sim$ 55%) produced particles with net positive charge. The silica content of ash produced during the second explosive period increased from 62% to 67% over the course of the eruptive period, and samples with similar silica content typically charged negatively in *James et al.*'s [2000] study, in disagreement with the LMA evidence of net positive charge. *Forward et al.* [2009] found that in contact electrification experiments using clear soda lime glass larger particles tend to charge positively, which is in line with the LMA observations. This may suggest that contact electrification was the dominant mechanism, but further laboratory work is needed to gain a better understanding of the roles of these charging mechanisms.

Though monopolar structures were most commonly inferred in the Eyjafjallajökull data, it is likely that there was also an upper negative charge region that was simply undetectable in the lightning data or was not always electrified enough to be involved in the electrical activity. Two or more charge regions have been commonly inferred from other volcanic lightning/electrification studies (e.g., *Lane and Gilbert* [1992], positive over negative; *Hoblitt* [1994], positive over negative; *McNutt and Davis* [2000], positive over negative; *Miura et al.* [2002], positive over negative over positive; *Thomas et al.* 2010], polarities not determined; *Behnke et al.* [2013], polarities not determined), so, for multiple charge regions to be uncommon in the Eyjafjallajökull data is somewhat surprising. Note that some of these studies used surface electric field measurements, which does not provide a unique solution to the charge structure like the LMA; however, the LMA does not show the complete charge structure. The LMA does not show weakly electrified regions where electrical activity does not occur, though weakly electrified regions would also be difficult to infer from surface electric field measurements. Regardless, the infrequent inference of an upper negative charge region suggests that it was weakly electrified and was thus not having a large impact on the lightning morphology. Multiple charge regions would be expected to form as a result of gravitational sedimentation of oppositely charged ejecta, as *Lane and Gilbert* [1992] and *Miura et al.* [2002] concluded, though a

dipolar or tripolar structure would also form as a result of plume-based ice-contact charging as long as the thermodynamic conditions in the plume were conducive to it.

The arguments in favor of vent charging explain why lightning was occurring low in altitude, but it does not adequately explain why there was not very much lightning during the beginning of the second explosive period (5–10 May), shown in Figure 2a. One could use plume height as a proxy for eruptive vigor and argue that the overall lower plume heights observed from 5 to 10 May (Figure 2b) show that the eruption was not as strong during this period and thus less vent charging would be expected, but this argument is not valid for two reasons. First, there are many instances where the plume height from 11 to 21 May was comparable to or lower than the plume height from 5 to 10 May, yet high rates of lightning occurred. Examples of this are 11–13 May, 15 May, and 18–21 May. Second, high wind speeds from 5 to 10 May (Figure 2c) were likely to have suppressed the plume height, making plume height a poor proxy for eruptive vigor. The plume height data do not show convincing evidence that a change in the eruption strength caused the onset of lightning on 11 May.

There is evidence that meteorological conditions changed during the second explosive period, which could have caused plume-based ice-contact charging to sufficiently electrify the plume for high rates of lightning to occur; however, as discussed above, the three-dimensional LMA observations do not support that conclusion. Figures 2a and 2b show a temporal correlation between lightning rate and isotherm height. The figure shows that it was significantly warmer during 5–10 May, when very little lightning was observed, than it was from 11 to 21 May, when high rates of lightning were observed (with the exception of a brief increase in temperature on 12 May). This correlation has already been described by *Arason et al.* [2011c], who compared plume top temperatures (derived by comparing the radar data to the atmospheric data from the UM) to the ATDnet-detected lightning rates and found that higher rates of lightning occurred with decreasing plume top temperatures. This led *Arason et al.* [2011c] to conclude that plume-based ice-contact charging was likely responsible for the lightning detected by ATDnet. They noted that ATDnet would have been detecting primarily large-scale lightning discharges and that the smaller discharges that one can see near the vent in photographs of the eruption were likely caused by a vent charging mechanism, which ATDnet was not likely to have detected due to their small extent. However, the LMA observations indicate that even the large-scale lightning discharges appear to have initiated near the vent where vent charging was occurring (e.g., Figures 7, 8, 11, and 15).

If ice-contact charging was having a significant effect on the electrification, then one would expect to see lightning initiating at higher altitudes in the plume, where it would be cold enough for ice-ice collisions to occur. Because the threshold field for electrical breakdown decreases exponentially with decreasing air density, lower electric fields and thus lower charge densities are required for lightning initiation at higher altitudes. In effect, it is "easier" to initiate lightning at high altitudes than low altitudes. There is little to no evidence of discharges initiating in a high field region between the negative and positive charge regions, but, as noted earlier, not all of the discharges are well understood. Perhaps a full 12-station LMA network would have revealed more details on the morphology of discharges, showing more complexity in the charge structure and offer more clues about the role of ice-contact charging. Note that the lack of upper level initiations does not necessarily rule out the possibility of ice-contact charging, but it does suggest that it was weak. It is also possible that the upper part of the positive charge region was being sufficiently discharged by lightning to keep the upper level electric field below the threshold for initiation. Nevertheless, the existing data support the conclusion that vent charging was the dominant charging mechanism in the plume of Eyjafjallajökull during the second explosive period but do not explain why lightning suddenly "turned on" on 11 May 2010.

6. Conclusions

The six-station Lightning Mapping Array data obtained during the 2010 eruption of Eyjafjallajökull show that moderate amounts of lightning occurred in the plume of Eyjafjallajökull during the latter part (11–21 May) of the second explosive period (5–22 May). Peak flash rates of small and regular discharges were 150 and 50 discharges per hour, which is relatively low compared to previous LMA studies of lightning during the 2009 eruption of Redoubt Volcano, where peak flash rates of regular discharges were on the order of 100 per minute.

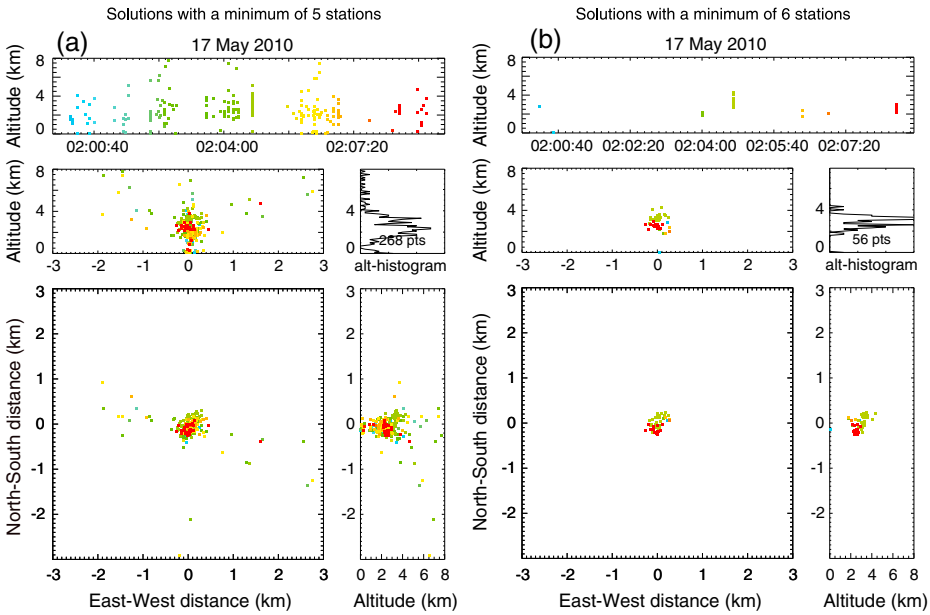

Figure A1. (a) Ten minutes of processed LMA data from 01:59 to 02:09 UTC on 17 May 2010, showing all solutions located by a minimum of five stations. (b) Same as Figure A1a, but showing only the solutions located by all six stations.

Single-station observations revealed that in addition to discrete lightning discharges, continuous RF electrical activity was observed during the first explosive period (14–18 April). No continuous RF electrical activity was observed during the second explosive period, perhaps due to variations in the eruption strength or type (magmatic as opposed to phreatomagmatic). Further study is needed to clarify the link between eruptive processes and the occurrence of continuous RF.

The three-dimensional lightning mapping data obtained during the second explosive period clearly showed a dominant, low-altitude region of positive charge in the plume. A negative-over-positive dipolar structure was observed infrequently. The data showed that electrical activity was most concentrated near the vent due to vent charging. The charge structure results indicate that the ejecta carried a net positive charge. Further laboratory work is needed to understand the roles of the various vent charging mechanisms in producing charged particles.

It is not clear why so little lightning was observed from 5 to 10 May yet relatively high-rates of lightning were observed from 11 to 21 May, and this remains an open question for future research. The abrupt onset of lightning on 11 May suggests that there might have been a corresponding abrupt change in a process relating to the charging mechanisms, such as an increase in eruptive vigor leading to enhanced vent charging or a change in atmospheric conditions that would facilitate plume-based ice-contact charging. Plume height measurements are the only available indicator of eruptive strength, and in this case they do not offer clear evidence that there was a significant change in the eruption. The meteorological data show that the 11–21 May period was approximately 10° colder than the 5–10 May period, but the morphology of the lightning flashes does not show evidence that ice-contact charging was significantly contributing to the electrification.

Appendix A: LMA Data-Filtering Methods

In order to maximize the number of solutions from the LMA measurements, the data were processed by requiring a minimum of five of the six stations to participate in the solutions as opposed to the minimum of six that is usually used. This requirement allows for solutions to be found from any combination of five of the six stations as well as for solutions from all six stations. An unwanted side effect of requiring a minimum of five stations instead of requiring all six is that it substantially increases the number of noise-contaminated solutions. The large amount of noise in the processed data made it difficult to calculate reliable flash rates, so the data were filtered by limiting the range of the five- and six-station solutions to reduce the noise.

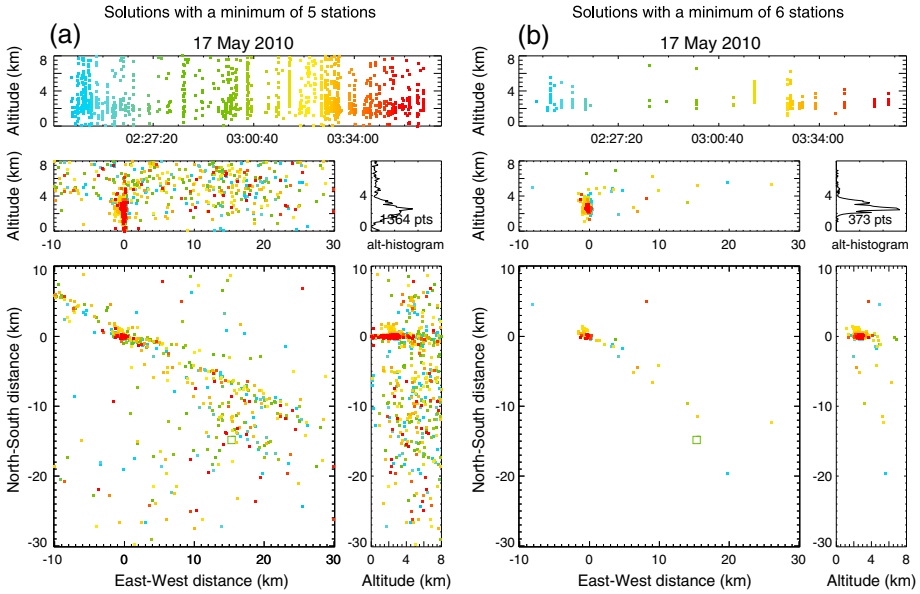

Figure A2. (a) Two hours of processed LMA data from 01:54 to 03:54 UTC on 17 May 2010, showing all solutions located by a minimum of five stations. (b) Same as Figure A2a, but showing only the solutions located by all six stations.

The main reason to use the five-station solutions was to include the small, short duration discharges that occurred over the vent frequently throughout the eruption that were commonly missed by one of the stations. An example of the difference between the five- and six-station data is shown in Figure A1. The data shown in Figure A1a contain all of the five- and six-station solutions in the region shown. The data shown in Figure A1b contain only the six-station solutions. There were 212 more solutions (about 5 times as many) in the five-station data than the six-station data. The far eastern Hraun station was the one station that missed most of these radiation sources, likely due to its distance from the volcano (80 km). In fact, of the 212 sources in Figure A1 that were located by only five stations, Hraun participated in the solutions of only 16 of these sources.

Though there are more well-located solutions in the five-station data, there is also much more noise. Figure A2 compares 2 h of five- and six-station data over a 40 km by 40 km region, which is the region in which all of the lightning in the entire data set occurred. No lightning was ever observed outside of this region. Away from the vent, located at the coordinate origin $(0, 0)$ in Figure A2, there was a significant amount of scattered noise solutions in the five-station data (Figure A2a), which mostly disappear if only the six-station data are displayed (Figure A2b). Thus, the six-station data are better for reducing noise, though the five-station data have more well-located solutions.

In order to make a data set that had the benefits of both the five- and six-station solutions, a hybrid of the five- and six-station data set was used. The advantage of the five-station data is that it retains the small discharges that occurred over the vent, but its disadvantage is the larger amount of noise. The six-station data have less noise, but it excludes most of the small, over-the-vent discharges. The data were hybridized by excluding all five-station solutions that were outside a 3 km by 3 km region centered on the vent and excluding all six-station solutions that were outside of a 40 km by 40 km region centered around the coordinates $(10, -10)$ in Figure A2. Further, in both cases the maximum χ^2_ν value was set to 5 assuming 30 ns timing errors and sources were excluded if they had altitudes lower than 1.5 km or higher than 8 km. By limiting the five-station solutions to a small range, well-located five-station solutions outside of the region were excluded from the hybrid data set in addition to noise; however, this method is believed to offer the best compromise.

Acknowledgments
This work was supported by the U.S. National Science Foundation under grant ATM-0739085 and by the National Oceanic and Atmospheric Administration under grant NA11NES4400007. We thank the UK Met Office for the ATDnet lightning data. We thank the individuals who assisted us and hosted our instruments in Iceland. The manuscript was greatly improved by reviews from Edward Mansell, Earle Williams, and one anonymous reviewer.

References

Anderson, R., S. Björnsson, D. Blanchard, S. Gathman, J. Hughes, S. Jónasson, C. Moore, H. Survilas, and B. Vonnegut (1965), Electricity in volcanic clouds, *Science*, *148*(3674), 1179–1189.

Arason, P., G. N. Petersen, and H. Björnsson (2011a), Observations of the altitude of the volcanic plume during the eruption of Eyjafjallajökull April–May 2010, *Earth Syst. Sci. Data*, *3*, 9–17, doi:10.5194/essd-3-9-2011.

Arason, P., G. N. Petersen, and H. Björnsson (2011b), *Plume-Top Altitude Time-Series During 2010 Volcanic Eruption of Eyjafjallajökull*, Icelandic Meteorological Office, Reykjavik, doi:10.1594/PANGAEA.760690.

Arason, P., A. Bennett, and L. E. Burgin (2011c), Charge mechanisms of volcanic lightning revealed during the 2010 eruption of Eyjafjallajökull, *J. Geophys. Res.*, *116*, B00C03, doi:10.1029/2011JB008651.

Behnke, S. A., R. J. Thomas, P. R. Krehbiel, and S. R. McNutt (2012), Spectacular lightning revealed in 2009 Mount Redoubt eruption, *Eos Trans. AGU*, *93*(20), 193–194.

Behnke, S. A., R. J. Thomas, S. R. McNutt, D. J. Schneider, P. R. Krehbiel, W. Rison, and H. E. Edens (2013), Observations of volcanic lightning during the 2009 eruption of Redoubt Volcano, *J. Volcanol. Geotherm. Res.*, *259*, 214–234, doi:10.1016/j.jvolgeores.2011.12.010.

Bennett, A., P. Odams, D. Edwards, and P. Arason (2010), Monitoring of lightning from the April–May 2010 Eyjafjallajökull volcanic eruption using a very low frequency lightning location network, *Environ. Res. Lett.*, *5*(4), 44,013–44,022.

Blanchard, D. (1964), Charge separation from saline drops on hot surfaces, *Nature*, *201*, 1164–1166.

Brook, M., C. Moore, and T. Sigurgeirsson (1974), Lightning in volcanic clouds, *J. Geophys. Res.*, *79*(3), 472–475.

Bruning, E. C., W. D. Rust, D. R. MacGorman, M. I. Biggerstaff, and T. J. Schuur (2010), Formation of charge structures in a supercell, *Mon. Weather Rev.*, *138*, 3740–3761, doi:10.1175/2010MWR3160.1.

Coleman, L. M., T. C. Marshall, M. Stolzenburg, T. Hamlin, P. R. Krehbiel, W. Rison, and R. J. Thomas (2003), Effects of charge and electrostatic potential on lightning propagation, *J. Geophys. Res.*, *108*(D9), 4298, doi:10.1029/2002JD002718.

Dellino, P., M. T. Gudmundsson, G. Larsen, D. Mele, J. A. Stevenson, T. Thordarson, and B. Zimanowski (2012), Ash from the Eyjafjallajökull eruption (Iceland): Fragmentation processes and aerodynamic behavior, *J. Geophys. Res.*, *117*, B00C04, doi:10.1029/2011JB008726.

Dickinson, J. T., S. C. Langford, L. C. Jensen, G. L. McVay, J. F. Kelso, and C. G. Pantano (1988), Fractoemission from fused silica and sodium silicate glasses, *J. Vac. Sci. Technol. A*, *6*, 1084–1089.

Edens, H. E., et al. (2012), VHF lightning mapping observations of a triggered flash, *Geophys. Res. Lett.*, *39*, L19807, doi:10.1029/2012GL053666.

Forward, K. M., D. J. Lacks, and R. M. Sankaran (2009), Charge segregation depends on particle size in triboelectrically charged granular materials, *Phys. Rev. Lett.*, *102*, 028001.

Gudmundsson, M. T., et al. (2012), Ash generation and distribution from the April–May 2010 eruption of Eyjafjallajökull, Iceland, *Sci. Rep.*, *2*, 57, doi:10.1038/srep00572.

Hoblitt, R. (1994), An experiment to detect and locate lightning associated with eruptions of Redoubt Volcano, *J. Volcanol. Geotherm. Res.*, *62*, 499–517.

Houghton, I. M. P., K. L. Aplin, and K. A. Nicoll (2013), Triboelectric charging of volcanic ash from the 2011 Grímsvötn eruption, *Phys. Rev. Lett.*, *111*, 118501.

James, M. R., S. J. Lane, and J. S. Gilbert (2000), Volcanic plume electrification—Experimental investigation of fracture-charging mechanism, *J. Geophys. Res.*, *105*, 16,641–16,649.

James, M. R., L. Wilson, S. J. Lane, J. S. Gilbert, T. A. Mather, R. G. Harrison, and R. S. Martin (2008), Electrical charging of volcanic plumes, *Space Sci. Rev.*, *137*, 399–418.

Krehbiel, P. R., J. A. Riousset, V. P. Pasko, R. J. Thomas, W. Rison, M. A. Stanley, and H. E. Edens (2008), Upward electrical discharges from thunderstorms, *Nat. Geosci.*, *1*, 233–237.

Lacks, D. J., and R. M. Sankaran (2011), Contact electrification of insulating materials, *Phys. D.: Appl. Phys*, *44*(45), 453001, doi:10.1088/022-3727/44/45/453001.

Lane, S. J., and J. S. Gilbert (1992), Electric potential gradient changes during explosive activity at Sakurajima Volcano, Japan, *Bull. Volcanol.*, *54*, 590–594.

Marshall, T. C., M. Stolzenburg, C. Maggio, L. M. Coleman, P. R. Krehbiel, T. Hamlin, R. J. Thomas, and W. Rison (2005), Observed electric fields associated with lightning initiation, *Geophys. Res. Lett.*, *32*, L03813, doi:10.1029/2004GL021802.

McNutt, S. R., and C. Davis (2000), Lightning associated with the 1992 eruptions of Crater Peak, Mount Spurr Volcano, Alaska, *J. Volcanol. Geotherm. Res.*, *102*, 45–65.

Miura, T., T. Koyaguchi, and Y. Tanaka (2002), Measurements of electric charge distribution in volcanic plumes at Sakurajima Volcano, Japan, *Bull. Volcanol.*, *64*, 75–93.

Morton, B. R., G. Taylor, and J. S. Turner (1956), Turbulent gravitational convection from maintained and instantaneous sources, *Philos. Trans. R. Soc. London A*, *234*(1196), 1–23, doi:10.1098/rspa.1956.0011.

Newhall, C., and S. Self (1982), The volcanic explosivity index (VEI): An estimate of explosive magnitude for historical volcanism, *J. Geophys. Res.*, *87*(C2), 1231–1238.

Riousset, J. A., V. P. Pasko, P. R. Krehbiel, R. J. Thomas, and W. Rison (2007), Three-dimensional fractal modeling of intracloud lightning discharge in a New Mexico thunderstorm and comparison with lightning mapping observations, *J. Geophys. Res.*, *112*, D15203, doi:10.1029/2006JD007621.

Rison, W., R. J. Thomas, P. R. Krehbiel, T. Hamlin, and J. Harlin (1999), A GPS-based three-dimensional lightning mapping system—Initial observations, *Geophys. Res. Lett.*, *26*, 3573–3576.

Rust, W. D., D. R. MacGorman, E. C. Bruning, S. A. Weiss, P. R. Krehbiel, R. J. Thomas, W. Rison, T. Hamlin, and J. Harlin (2005), Inverted-polarity electrical structures in thunderstorms in the Severe Thunderstorm Electrification and Precipitation Study (STEPS), *Atmos. Res.*, *76*, 247–271, doi:10.1016/j.atmosres.2004.11.029.

Shao, X. M., and P. R. Krehbiel (1996), The spatial and temporal development of intracloud lightning, *J. Geophys. Res.*, *101*(D21), 26,641–26,668.

Sparks, R. S. J., M. I. Bursik, S. N. Carey, J. S. Gilbert, L. S. Glaze, H. Sigurdsson, and A. W. Woods (1997), *Volcanic Plumes*, pp. 97–101, John Wiley, New York.

Tessendorf, S. A., S. A. Rutledge, and K. C. Wiens (2007a), Radar and lightning observations of normal and inverted polarity multicellular storms from STEPS, *Mon. Weather Rev.*, *135*, 3682–3706, doi:10.1175/2007MWR1954.1.

Tessendorf, S. A., K. C. Wiens, and S. A. Rutledge (2007b), Radar and lightning observations of the 3 June 2000 electrically inverted storm from STEPS, *Mon. Weather Rev.*, *135*, 3665–2681, doi:10.1175/2006MWR1953.1.

Thomas, R. J., P. R. Krehbiel, W. Rison, T. Hamlin, J. Harlin, and D. Shown (2001), Observations of VHF source powers radiated by lightning, *Geophys. Res. Lett.*, *28*(1), 143–146.

Thomas, R. J., S. A. Behnke, T. Hamlin, J. Harlin, P. R. Krehbiel, and W. Rison (2002), New Mexico thunderstorms observed by the Lightning Mapping Array: An overview of one season, *Eos Trans. AGU*, *83*(47), Fall Meet. Suppl., Abstract A71B–0097.

Thomas, R. J., P. R. Krehbiel, W. Rison, J. Harlin, T. Hamlin, and N. Campbell (2003), The LMA flash algorithm, *Proceedings of the 12th International Conference on Atmospheric Electricity—ICAE*, ICAE, Versailles.

Thomas, R. J., P. R. Krehbiel, W. Rison, S. Hunyady, W. P. Winn, T. Hamlin, and J. Harlin (2004), Accuracy of the Lightning Mapping Array, *J. Geophys. Res.*, *109*, D14207, doi:10.1029/2004JD004549.

Thomas, R. J., P. R. Krehbiel, W. Rison, H. E. Edens, G. D. Aulich, W. P. Winn, S. R. McNutt, G. Tytgat, and E. Clark (2007), Electrical activity during the 2006 Mount St. Augustine volcanic eruptions, *Science*, *315*, 1097.

Thomas, R. J., S. R. McNutt, P. R. Krehbiel, W. Rison, G. Aulich, H. E. Edens, G. Tytgat, and E. Clark (2010), Lightning and electrical activity during the 2006 eruption of Augustine Volcano, in *The 2006 Eruption of Augustine Volcano, Alaska*, edited by J. Powers et al., pp. 579–608, U.S Geological Survey Professional Paper 1769.

Wiens, K. C., S. A. Rutledge, and S. A. Tessendorf (2005), The 29 June 2000 supercell observed during STEPS. Part II: Lightning and charge structure, *J. Atmos. Sci.*, *62*, 4151–4177.

Williams, E. R., and S. R. McNutt (2005), Total water contents in volcanic eruption clouds and implications for electrification and lightning, in *Recent Progress in Lightning Physics*, edited by C. Pontikis, pp. 81–94, Research Signpost, Kerala, India.

Williams, E. R., C. M. Cooke, and K. A. Wright (1985), Electrical discharge propagation in and around space charge clouds, *J. Geophys. Res.*, *90*, 6054–6070.

Woodhouse, M. J., A. J. Hogg, J. C. Phillips, and R. S. J. Sparks (2013), Interaction between volcanic plumes and wind during the 2010 Eyjafjallajökull eruption, Iceland, *J. Geophys. Res. Solid Earth*, *118*, 1–18, doi:10.1029/2012JB009592.